

Thieno[2,3-*d*]pyrimidine-2,4(1*H*,3*H*)-dione Derivative Inhibits D-Dopachrome Tautomerase Activity and Suppresses the Proliferation of Non-Small Cell Lung Cancer Cells

Zhangping Xiao, Angelina Osipyan, Shanshan Song, Deng Chen, Reinder A. Schut, Ronald van Merkerk, Petra E. van der Wouden, Robbert H. Cool, Wim J. Quax, Barbro N. Melgert, Gerrit J. Poelarends, and Frank J. Dekker*



Cite This: *J. Med. Chem.* 2022, 65, 2059–2077



Read Online

ACCESS |



Metrics & More

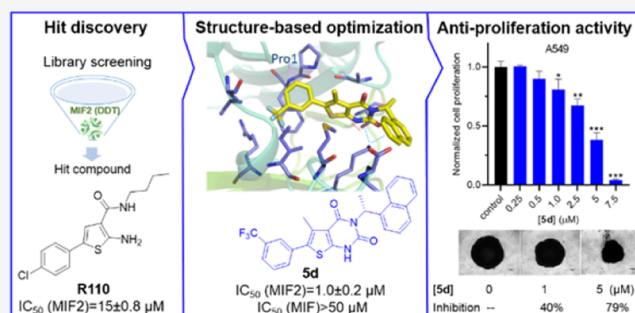


Article Recommendations



Supporting Information

ABSTRACT: The homologous cytokines macrophage migration inhibitory factor (MIF) and D-dopachrome tautomerase (D-DT or MIF2) play key roles in cancers. Molecules binding to the MIF tautomerase active site interfere with its biological activity. In contrast, the lack of potent MIF2 inhibitors hinders the exploration of MIF2 as a drug target. In this work, screening of a focused compound collection enabled the identification of a MIF2 tautomerase inhibitor R110. Subsequent optimization provided inhibitor **5d** with an IC_{50} of 1.0 μ M for MIF2 tautomerase activity and a high selectivity over MIF. **5d** suppressed the proliferation of non-small cell lung cancer cells in two-dimensional (2D) and three-dimensional (3D) cell cultures, which can be explained by the induction of cell cycle arrest via deactivation of the mitogen-activated protein kinase (MAPK) pathway. Thus, we discovered and characterized MIF2 inhibitors (**5d**) with improved antiproliferative activity in cellular models systems, which indicates the potential of targeting MIF2 in cancer treatment.



INTRODUCTION

Cancer is one of the major public health challenges and contributes to a currently estimated annual death toll of 10 million worldwide.¹ Although targeted cancer treatment has achieved enormous progress over the last decades, its effectiveness is limited by the heterogeneity and acquired therapy resistance of cancers.² Therefore, it is important to explore novel anticancer drug targets and to develop new therapeutic agents to target them. This could expand the possibilities to employ targeted therapeutic approaches and also increase the possibilities to develop combination therapy regimens.³ The macrophage migration inhibitory factor (MIF) family proteins are implicated in the development of cancers, which is demonstrated by the overexpression of MIF family proteins in several cancer types, such as genitourinary cancer,⁴ melanoma,⁵ neuroblastoma,⁶ and lung carcinoma.⁷ Notably, downregulation of MIF family proteins by gene-knockout⁸ or gene-knockdown^{9,10} exhibited reduction of tumor progression and induction of antitumor immune responses. Thus, MIF family proteins could be promising targets of novel cancer therapeutics.

The most studied member of the MIF family proteins is macrophage migration inhibitory factor (MIF), which was initially discovered as an inflammatory cytokine. Currently,

there is accumulating evidence revealing a key role in the proliferation of cancer cells. MIF exerts its proliferative effect through various mechanisms, for example, binding to the cognate receptor cluster of differentiation 74 (CD74).^{11,12} CD74 binding induces the activation of the MAPK pathway, which stabilizes cyclin D1 and consequently regulates cell cycle progression to enhance cell proliferation. In addition, activation of the MAPK pathway also suppresses p53 activity, which results in the inhibition of cell apoptosis.⁴ Other binding partners of MIF, such as CXCR4¹³ and JAB1 also play central roles in cancer growth. Several MIF-targeting reagents showed substantial potency on the deactivation of MIF-related signaling pathway and the inhibition of cancer cell proliferation.^{14,15}

D-Dopachrome tautomerase (D-DT or MIF2) is a structural and functional homologue but not a backup of MIF.¹⁶ Most studies on MIF2 were comparisons with MIF, as MIF2 is a

Received: September 10, 2021

Published: January 18, 2022



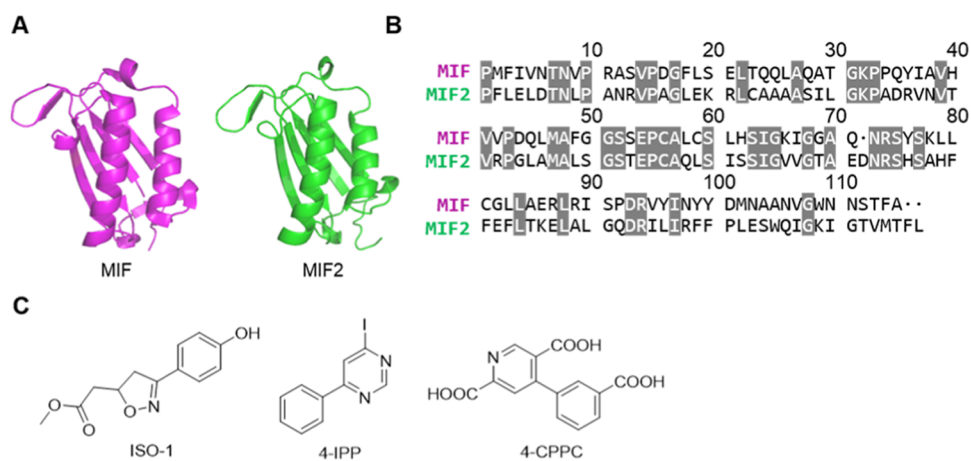


Figure 1. Tertiary and secondary structures of MIF and MIF2 and some key inhibitors. (A) Similar 3D structures of MIF (PDB code: 3ijj)³¹ and MIF2 (PDB code: 6c5f)³² monomers. (B) Comparison of the MIF and MIF2 amino acid sequences. (C) Some representative MIF or MIF2 tautomerase inhibitors. ISO-1 is one of the most studied MIF inhibitors.²⁵ 4-IPP is a covalent inhibitor for both MIF and MIF2.¹⁹ 4-CPPC is an MIF2 inhibitor with an IC_{50} value of 27 μ M with selectivity for MIF2 over MIF.³⁰

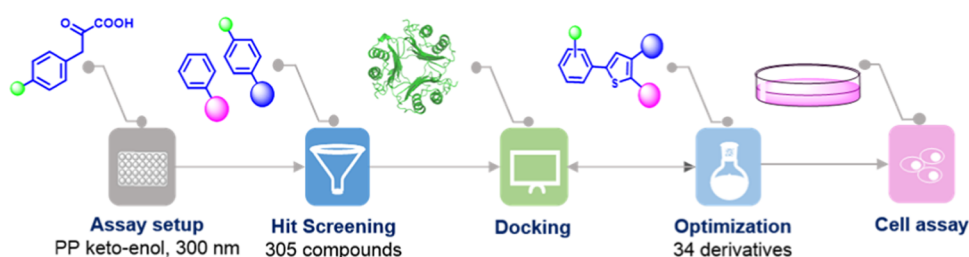


Figure 2. Workflow for the discovery of MIF2 inhibitors. In this study, a MIF2 tautomerase activity assay was established using phenylpyruvate as a substrate. This assay was employed to screen several structurally diverse compound collections. A hit compound was discovered and further optimized. The most potent MIF2 tautomerase inhibitor was also tested on non-small cell lung cancer cells for its effect on cell proliferation.

relatively recently identified family member of MIF.¹⁷ MIF2 and MIF share a high similarity in several aspects. The 3D structure shows that the overall folding and subunit topology of MIF2 and MIF are almost identical, with two β - α - β motifs related by *pseudo*-2-fold symmetry and similar trimeric β -sheet packing (Figure 1A).¹⁸ Both MIF2 and MIF harbor enzyme activity and catalyze the keto-enol tautomerization of 4-hydroxyphenylpyruvate (4-HPP) in an active site centered around proline-1. Moreover, both MIF and MIF2 are ligands of CD74 and JAB1¹⁷ that could consequently endow these two proteins with a similar effect on cell growth and tumorigenesis. Despite their high structure similarity, MIF and MIF2 share just 34% percent amino acid sequence identity (Figure 1B).¹⁹ These sequence differences may provide differences in interaction sites. For instance, the difference of amino acids inside the tautomerase active sites causes differences in their activity toward the keto-enol tautomerization of 4-HPP.¹⁷ Moreover, MIF2 does not bind to MIF receptors CXCR2/4 because it lacks a *pseudo*(E)LR motif, which mediates the interactions.^{20,21} Thus, understanding the similarities and differences between MIF2 and MIF is important for the discovery of therapeutics to selectively target these MIF family members.

Considerable efforts have been devoted to the discovery of small-molecule inhibitors to target MIF family proteins in cancers. For the last two decades, researchers have reported dozens of MIF-targeting inhibitors, most of which bind to the tautomerase active site of MIF. As the tautomerase active sites are located in close proximity to amino acid residues playing

key roles in binding to the CD74 receptor,^{22,23} small-molecule binders of the MIF tautomerase site can also interfere with the structural or dynamic features of MIF that are essential for CD74 binding and MIF-related cell signaling.²⁴ For instance, the most widely investigated MIF inhibitor ISO-1 (Figure 1C) not only inhibits MIF tautomerase activity²⁵ but also shows significant suppression of prostate cancer growth in cellular and animal models, which can be explained by the attenuation of MIF-triggered activation of the MAPK pathway.²⁶ In a recent study, we demonstrated that a 7-hydroxycoumarin derivative can interfere with MIF-CD74 interaction through binding to the MIF tautomerase active site.¹⁵ Additionally, the Jorgensen Lab discovered several promising biaryltriazole- or pyrazole-containing MIF inhibitors, which showed inhibitory potency at the nanomolar level.^{27,28} Moreover, we developed a potent MIF-targeted proteolysis targeting chimera (PROTAC) to remove the MIF protein from its interaction network, which further expanded the toolbox to study MIF functions.²⁹ However, little is known about the effect of MIF2 inhibitors on cancer development due to a lack of potent MIF2 inhibitors and other effective molecular tools. 4-Iodo-6-phenylpyrimidine (4-IPP) is the firstly discovered MIF2 inhibitor, which covalently binds to proline-1 of MIF2 to interfere with its tautomerase enzyme activity and its biological function.¹⁹ However, 4-IPP shows low potency on MIF2 inhibition with an IC_{50} value larger than 100 μ M. In contrast, 4-IPP inhibits MIF with micromolar potency and binds covalently to the active site proline. As reported in 2019, Bucala and co-workers discovered the selective MIF2 inhibitor 4-(3-carboxyphenyl)-

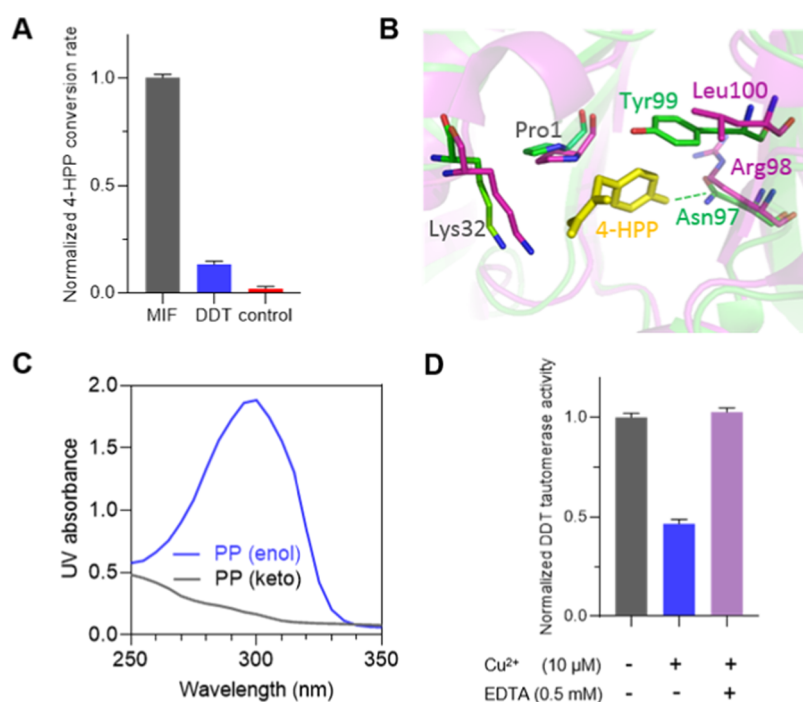


Figure 3. Setup of the phenylpyruvate tautomerization-based MIF2 binding assay. (A) Rate of the MIF- or MIF2-catalyzed 4-HPP tautomerization reaction. The rate of the MIF-catalyzed reaction is 10-fold faster than that of the MIF2-catalyzed reaction.¹⁷ (B) Superposition of MIF2 (PDB code: 6cSf)³² and complex (PDB: 6ijj)³¹ of MIF and 4-HPP reveals the differences in the tautomerase active site pocket. (C) UV spectra of 1 mM phenylpyruvate in its keto-form (gray) or enol-form (blue). (D) The signal in the MIF2 tautomerase activity assay is halved in the presence of 10 μM Cu^{2+} and can be rescued by 0.5 mM ethylenediamine tetraacetic acid (EDTA).

Table 1. Enzyme Kinetic Parameters for the Conversion of PP and Its Derivatives by MIF and MIF2

enzyme	parameter	PP	4-CPP	4-HPP	4-MPP
MIF	K_M (mM)	0.76 ± 0.28	0.60 ± 0.24	0.94 ± 0.14	1.3 ± 0.32
	k_{cat} (s^{-1}) [#]	14 ± 2.5	25 ± 4.1	25 ± 1.8^{37}	13 ± 1.7
	k_{cat}/K_M ($10^4 \text{ M}^{-1} \text{ s}^{-1}$)	1.9	4.3	2.6	0.98
MIF2	K_M (μM)	2.4 ± 0.56	2.17 ± 0.22	3.62 ± 0.47	6.7 ± 0.78
	k_{cat} (s^{-1})	132 ± 17	68 ± 3.7	13 ± 1.0	28 ± 2.3
	k_{cat}/K_M ($10^4 \text{ M}^{-1} \text{ s}^{-1}$)	5.5	3.2	0.37	0.43

2,5-pyridinedicarboxylic acid (4-CPDC) through virtual screening, which displays an IC_{50} value of 27 μM on MIF2 tautomerase activity.³⁰ More importantly, 4-CPDC can also inhibit MIF2-CD74 binding and MIF2-mediated pERK activation. To further investigate the biological role of MIF2 in cancer and exploit it to develop cancer therapy, more potent MIF2 selective inhibitors are needed.

In this study, we describe the discovery and exploration of a potent and selective MIF2 inhibitor **5d** with a low micromolar-level potency for inhibition of both MIF2 tautomerase activity and cancer cell proliferation (Figure 2). First, the tautomerase activity assay was optimized for assessing the potency of MIF2 inhibitors in competition binding studies and enzyme kinetic analysis. Subsequently, several in-house available compound collections were screened and a promising hit compound was chosen for further optimization. Toward this aim, 33 analogues were prepared and tested for their inhibitory potency on MIF2 tautomerase activity. The most potent inhibitor **5d** was tested

in two-dimensional (2D) and three-dimensional (3D) cultures of non-small cell lung cancer (NSCLC) cell lines. Altogether, the development of **5d** provides a powerful tool for MIF2-oriented research and provides a perspective toward MIF2-directed therapeutics.

RESULTS

Optimization MIF2 Tautomerase Activity Assay. To facilitate the effective assessment of binding potency of MIF2 inhibitors, a convenient and reliable assay is needed. The most widely used assay to evaluate MIF tautomerase activity inhibition is the 4-HPP-based tautomerization assay, in which the potency on inhibition of MIF-catalyzed 4-HPP tautomerization is applied to reflect the binding affinity of the tested compound to MIF.³³ This assay was also applied to assess MIF2 binding in previous studies.³⁰ However, the catalytic activity of MIF2 on the 4-HPP keto-enol conversion is 10 times lower compared to MIF (Figure 3A).¹⁷ This renders

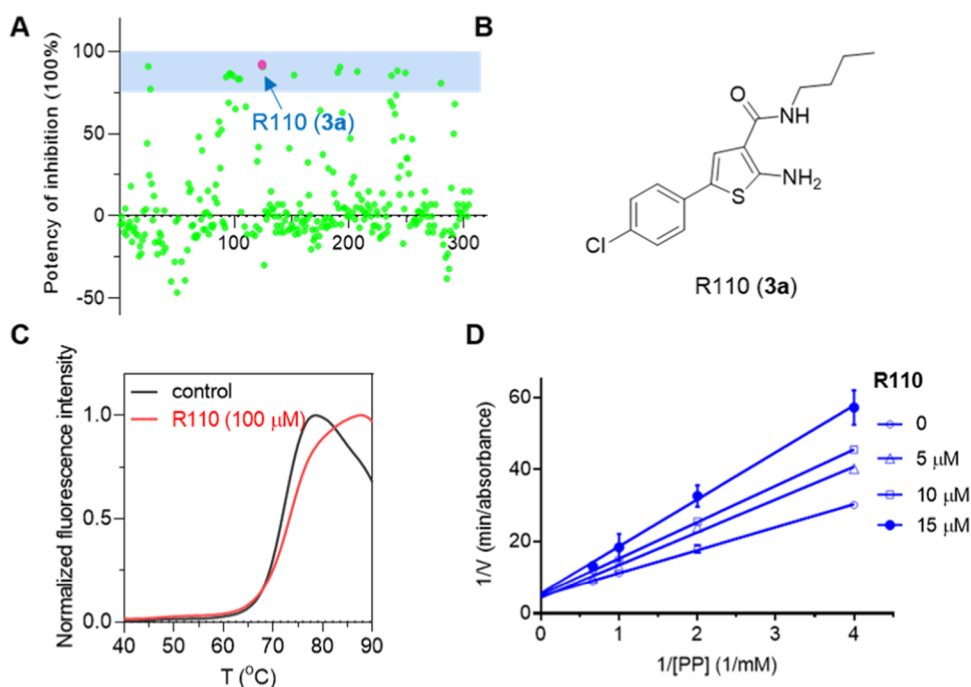


Figure 4. Library screening and hit confirmation. (A) 305 compounds from an in-house library were screened at a single concentration of 50 μM for their inhibition on MIF2 tautomerase activity. The inhibition potency of each compound was shown as an average of three measurements. (B) Structure of selected hit compound R110 (3a). (C) Fluorescence-based thermal shift assay result from the interaction between R110 and MIF2. ΔT_m depicts the difference between the apparent melting temperature of MIF2 with or without R110. (D) Lineweaver–Burk plot of MIF2 activity in the presence of R110 (3a). Results are shown as mean \pm standard deviation (SD) of three experiments.

4-HPP unsuitable as a substrate in the MIF2 tautomerase activity assay because high enzyme concentrations and long measurement times are needed. This indicates the need for a different substrate.

The structural features of the tautomerase active site of MIF2 were compared to the tautomerase active site of MIF. A superimposition of the crystal structure of MIF2³² on a complex³¹ of MIF and 4-HPP showed that the proline-1 of MIF2 overlaps well with the proline-1 of MIF, which indicates that the catalytic centers of MIF2 and MIF occupy the same spatial location in the active sites. Nevertheless, MIF2 is not able to form the two hydrogen bonds observed between Asn97 of MIF and the 4-position hydroxyl group of 4-HPP, as the Arg98 locates at the corresponding position of MIF2 (Figure 3B). Accordingly, we hypothesized that MIF2 could exhibit different catalytic activity for keto-enol tautomerization of 4-HPP analogues with different substituents at the phenyl 4-position. Therefore, we set out to find a more active substrate for MIF2 to establish a convenient and sensitive enzymatic assay. Three 4-HPP analogues, 4-methoxyphenylpyruvate (4-MPP), 4-chlorophenylpyruvate (4-CPP), and phenylpyruvate (PP), were synthesized and the catalytic activities of MIF and MIF2 toward these “artificial substrates” were tested. The measured parameters show that K_M values of MIF on catalyzing PP, 4-CPP, 4-HPP, and 4-MPP keto-enol conversion are 0.76, 0.60, 0.94, and 1.3 mM (Table 1), respectively. These values are lower than the corresponding values of MIF2. Nevertheless, the catalytic efficiencies for MIF and MIF2 on each substrate are diverse. For instance, the catalytic efficiency of MIF on 4-HPP is 7 times higher than that of MIF2, making 4-HPP a less effective MIF2 substrate. In contrast, MIF2 can catalyze the keto-enol conversion of PP around 3 times more efficient than MIF, which provides MIF2

with the highest catalytic efficiency for PP among this series of substrates. Interestingly, PP is a known MIF2 substrate and MIF2 was even named as phenylpyruvate tautomerase (PPT II) because of this property as early as 1997.³⁴ Altogether, this identifies PP as a substrate for a MIF2 tautomerase assay.

Next, PP was used to establish the MIF2 tautomerase assay in the same way as done for MIF. In this assay format, a MIF2 solution in assay buffer was mixed with the compound stock solution and an aqueous EDTA solution followed by 10 min preincubation.³⁵ The assay was started by adding a PP solution to the inhibitor–enzyme mixture. In the final reaction mixture, there were 50 nM MIF2, 0.5 mM PP, 2.5% (v/v) dimethyl sulfoxide (DMSO), and variable concentrations of the inhibitor. The formation of the reaction product was monitored at 300 nm and corrected for the blank in which the enzyme was excluded (Figure 3C). The linear regression parameters were utilized to determine the inhibitory potency or IC_{50} using GraphPad Prism. The window coefficient (Z' -factor) of this optimized assay was determined as 0.75 in this setup, indicating that the quality of this assay is sufficient for application in medium- to high-throughput screenings (0.5–1).³⁶ Similar to MIF, we observed that Cu^{2+} ions interfere with this MIF2 tautomerase activity assay and that including EDTA in the assay buffer prevents this (Figure 3D).³⁵

Compounds Screening and Hit Confirmation. The MIF2 tautomerase activity assay was employed to screen an in-house available compound collection containing 305 distinct chemical entities at compound concentrations of 50 μM (Figure 4A and Supporting Table 1). The performance of the MIF2 activity assay in this screening campaign proved to be excellent with an average Z' factor (a screening window coefficient) of 0.87. The hit identification criterion was defined as beyond 75% inhibition (Table S1). The inhibitory potency,

potential binding efficiency, and drug-likeness were used to select hit compounds for follow-up investigation. R110 (**3a**) exhibited good inhibitory potency against MIF2 tautomerization activity ($IC_{50} = 15 \mu M$) and good ligand efficiency ($LE = 0.34$) (Figure 4B). To verify the binding between R110 (**3a**) and MIF2, the thermal stability assay was performed as an orthogonal assay. The apparent melting temperature (ΔT_m) of MIF2 increased with $2.5 \text{ }^\circ C$ in the presence of $100 \mu M$ R110 (**3a**) (Figure 4C), which confirms binding of R110 (**3a**) to MIF2. Subsequently, the enzyme kinetics for binding of R110 (**3a**) to MIF2 were investigated. The Lineweaver–Burk plots show intersection at the ordinate (y -axis), demonstrating that R110 (**3a**) binds in competition with the substrate phenylpyruvate to the MIF2 tautomerase active site (Figure 4D). Taken together, R110 (**3a**) is a competitive inhibitor of MIF2 tautomerase activity with micromolar potency, indicating that R110 (**3a**) is a promising chemical starting point for the development of a more potent MIF2 inhibitor.

Design and Synthesis. To rationalize the binding between R110 (**3a**) and MIF2, a docking study was performed by docking R110 (**3a**) into the crystal structure of MIF2 (PDB code: 6c5f).³² Modeling was performed using the software Discovery Studio 3.0. R110 (**3a**) was docked into the tautomerase active site of the crystal structure of MIF2 and enzyme-minimized (Figure 5). The five highest-scoring poses

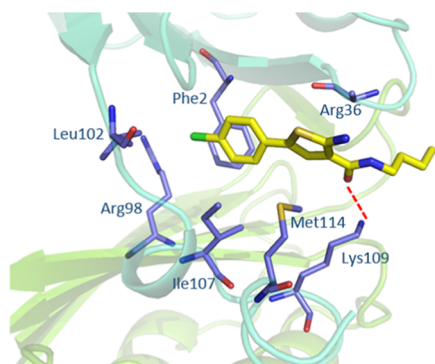


Figure 5. Schematic representation of the binding mode of R110 (**3a**) (thick sticks) with MIF2 (PDB code: 6c5f).³² The residues of the binding pocket are shown as thin sticks. The hydrogen bond formed with Lys109 is shown as the red dash line. Discovery Studio was employed for docking, and PyMOL was used for graph preparation.

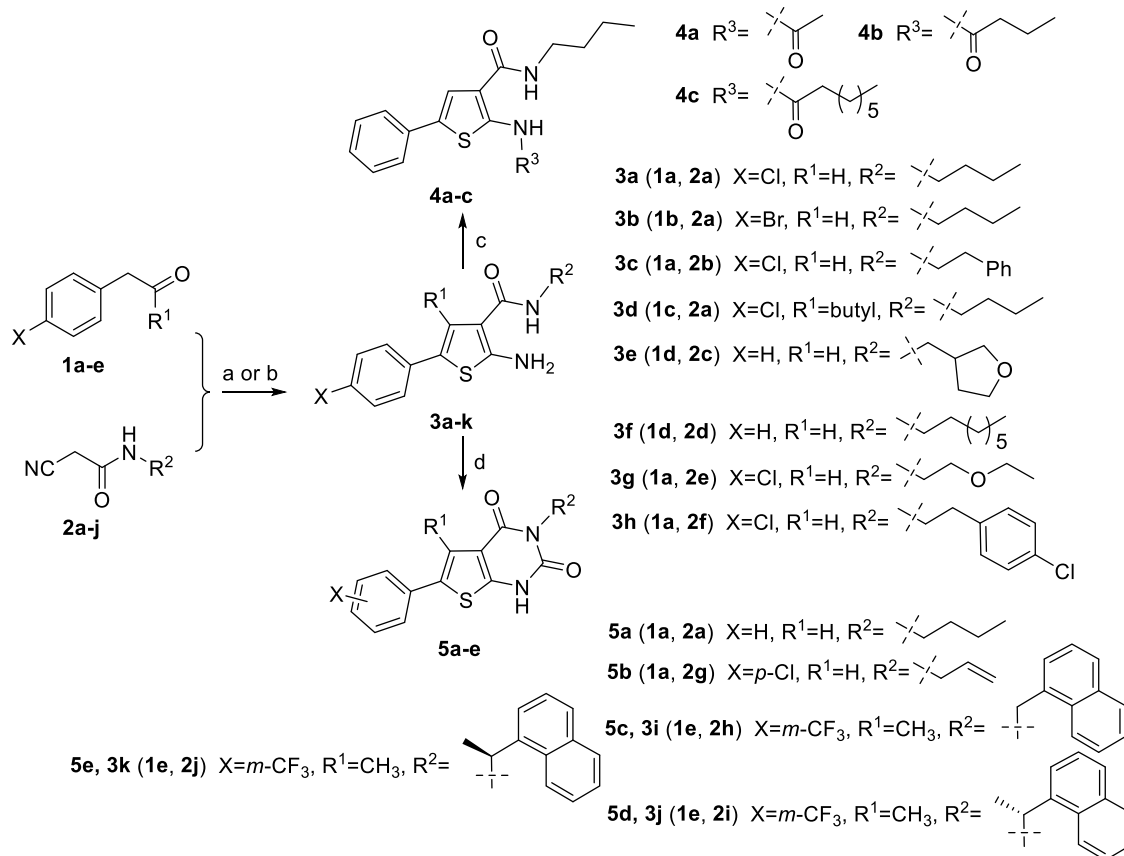
occupy similar positions. The optimal binding pose indicates that the chlorophenyl group of R110 (**3a**) is embedded into the hydrophobic active site pocket of MIF2, while the *n*-butyl group is exposed to water. The interactions between R110 (**3a**) and MIF2 are mainly formed through van der Waals forces, including the interactions between the chlorophenyl group and Phe2, Arg98, Leu102, and Ile107 of MIF2, and the interactions between the thiophene and Arg36, Met114 of MIF2. A hydrogen bond is formed between R110 (**3a**) and Lys109 of MIF2. This model indicates that there is still some unoccupied space around the chlorophenyl fragment and the butyl group of R110 (**3a**). Therefore, we set out to exploit these regions in our structure–activity relationship (SAR) with the aim to enhance the potency of the MIF2 inhibitor.

To optimize R110 (**3a**), phenylthiophene derivatives were constructed employing the Gewald three-component reaction as a key step using routes as depicted in scheme 1–3. Two different methods were employed to prepare compounds **3a**–

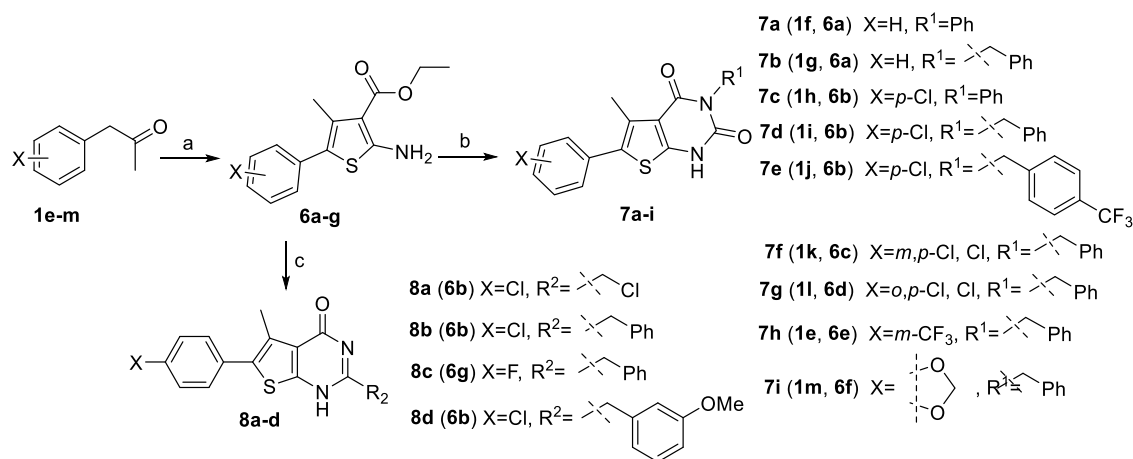
k. Compounds **3a**–**c** and **3e**–**h** were obtained using the Gewald-reaction employing different aldehydes, cyanoacetamides, and elementary sulfur as starting materials with yields of 18–56%. Compounds **3d** and **3i**–**k** were synthesized by condensation of the corresponding ketones and cyanoacetamides in the presence of $SnCl_4$ and Et_3N to provide the corresponding intermediates, which were cyclized with S_8 to afford the products with overall yields of 16–42%. The resulting 2-aminothiophenes were acylated by different acylchlorides to prepare the desired 2-amide-substituted thiophene products **4a**–**c** with yields of 44–58%. The 2-aminothiophenes were also employed to synthesize thieno[2,3-*d*]pyrimidine-2,4(1*H*,3*H*)-diones **5a**–**e** using 1,1'-carbonyldiimidazole (CDI) as a coupling reagent with yields of 40–91%. The profiles of **5d** were further investigated. **5d** and **5e** show different retention times on chiral chromatography and opposite optical rotation in optical characterization (Figure S3). The results together with the NMR spectra and high-resolution mass spectrometry (HRMS) data indicate that **5d** and **5e** are chirally pure enantiomers. The same scaffold in **7a**–**i** and **11a**–**b** was synthesized using a different method, in which the respective isocyanates were reacted with 2-aminothiophenes (**6a**–**g**) to the corresponding ureas that were cyclized by treatment with MeONa to provide overall yields of 20–62%. Compounds **8a**–**d** were constructed by the condensation of 2-aminothiophenes with nitriles in 4 N HCl to provide the corresponding products in yields of 32–60%. All final products were purified with chromatography, and their structures were characterized by 1H and ^{13}C NMR spectroscopy and liquid chromatography high-resolution mass spectrometry (LC-HRMS) (Supporting information). The purity of all tested compounds is >95% as determined by high-performance liquid chromatography (HPLC).

Structure–Activity Relationships. The inhibitory potency toward MIF2 tautomerase activity of this focused compound collection was evaluated using the MIF2 tautomerase activity assay to provide IC_{50} values as shown in Tables 2–4. The positive control compound 4-CPPC exhibits an IC_{50} of $47 \pm 7.2 \mu M$, which is in line with the result of $27 \mu M$ from the literature.³⁰ Compared with inhibitor **3a** (R110) with an IC_{50} of $15 \pm 0.8 \mu M$, the bromo-substituted analogue **3b** exhibits enhanced potency with an IC_{50} value of $7.2 \pm 0.6 \mu M$. Neither adding a butyl group to the 4-position of thiophene (**3d**) nor elongating the butyl to an octyl (**3f**) influenced the activity of R110 (**3a**). In contrast, replacement of butyl group with phenethyl (**3c**), (tetrahydrofuran-3-yl)methyl (**3e**), ethoxyethyl (**3g**), or 4-chlorophenethyl (**3h**) diminished the MIF2 inhibitory potency. Amidation of the 2-amino group with different acyls (**4a**–**c**) also failed to increase the potency. However, the derivatives with a CF_3 group and a naphthalene substitution (**3i**–**k**) showed increased activity, with an IC_{50} of $2.6 \pm 0.2 \mu M$ for the most potent compound **3i**.

To investigate the importance of the thiophene core of inhibitors, we changed the thiophene to thieno[2,3-*d*]pyrimidine-2,4(1*H*,3*H*)-diones using ring closure strategies to bridge the 2-amino and 3-amide functionalities. The activities of **5a** and **5b**, which have aliphatic chains at R^3 position, are similar to R110 (**3a**). By analyzing the SARs of **7a**–**d**, we observed that a chlorophenyl group, compared with a phenyl group, at the R^2 position and a benzyl group at the R^3 position is beneficial for MIF2 inhibitory potency within this series of inhibitors. Thus, **7d**, which has an IC_{50} of $5.1 \pm 0.5 \mu M$, was employed as a new starting point for further exploring the

Scheme 1. Synthesis of Thiophene Derivatives^{4f}

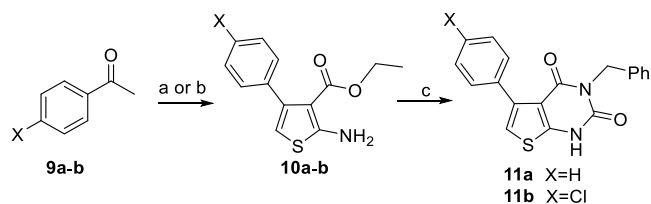
^{4f}Reagents and conditions: a. (i) S_8 , TEA, EtOH, reflux; b. (i) SnCl_4 , TEA, THF; (ii) S_8 , EtOH, TEA, reflux; c. Acyl chloride, pyridine, *N,N*-dimethylformamide (DMF), rt; d. CDI, CH_2Cl_2 .

Scheme 2. Synthesis of Thiophene Derivatives^{4g}

^{4g}Reagents and conditions: a. (i) Ammonium acetate, AcOH, toluene, reflux; (ii) S_8 , TEA, EtOH, reflux; b. (i) R-NCO, pyridine, reflux; (ii) 30% MeONa, reflux; c. R-CN, HCl, dioxane, reflux.

SARs. First, a CF_3 group installed on the *para*-position of the benzyl group afforded **7e**, which shows similar potency to **7d**. Subsequently, we moved the phenyl or 4-chlorophenyl group to the neighboring position to prepare **11a** and **11b**, which both show impaired activity. Therefore, we started again from **7d** to explore the space around the 4'-chlorophenyl group. Interestingly, all four patterns of substitutions (**7f**–**i**) on the phenyl ring provide increased potency. Among them, the 3'-

CF_3 substitution (**7h**) results in a 3-fold improvement of potency with an IC_{50} of $1.7 \pm 0.1 \mu\text{M}$. By replacing the benzyl group of **7h** with a (naphthalen-1-yl)methyl group, we achieved **5c**, which affords another a 2-fold increase of potency on MIF2 tautomerase inhibition with an IC_{50} of $0.8 \pm 0.1 \mu\text{M}$. However, the solubility of **5c** is only $3.3 \mu\text{g/mL}$ ($7.4 \mu\text{M}$), which would be a limitation for further application in cell-based assays. Therefore, we synthesized a pair of methyl-

Scheme 3. Synthesis of Thiophene Derivatives^a

^aReagents and conditions: a. Ethyl cyanoacetate, S₈, TEA, EtOH, reflux; b. (i) Ethyl cyanoacetate, acetic acid, toluene, reflux; (ii) S₈, EtOH, reflux; c. CDI, CH₂Cl₂.

branched enantiomers (**5d** and **5e**) to break the planarity of **5c** and to improve water solubility.³⁸ Favorably, both **5d** and **5e** have improved solubility in aqueous solution with saturated concentrations of 16 μg/mL (36 μM) and 15 μg/mL (33 μM)

for **5d** and **5e**, respectively. Moreover, **5d** exhibits a comparable potency as **5c**, while **5e** is less active. This identified **5d** as one of the most potent inhibitors of MIF2 tautomerase with a water solubility that is sufficient for further studies.

In addition, a scaffold hopping from thieno[2,3-*d*]-pyrimidine-2,4(1*H*,3*H*)-dione (**7d**) to thieno[2,3-*d*]-pyrimidin-4(1*H*)-one (**8b**) led to a decrease in potency with an IC₅₀ of 15 ± 1.4 μM (Table 4). Adding a methoxy group to the meta-position of benzyl (**8d**) increases the inhibitory potency of **8b** by 3 times to an IC₅₀ of 4.3 ± 0.4 μM, but modifying the benzyl to chloromethyl group (**8a**) or Cl to F (**8c**) failed to improve the potency of compound **8b**.

Characterization of 5d. We next confirmed that **5d** inhibits MIF2 through a direct interaction by monitoring MIF2 thermal stability using the thermal shift assay. Incubation with **5d** stabilizes MIF2 from heat-induced unfolding and increased

Table 2. Potency of MIF2 Tautomerase Inhibition by Thiophene Derivatives Determined Using the MIF2-Catalyzed PP Conversion Assay^a

	X	R ¹	R ²	R ³	IC ₅₀ (μM) [#]
4-CPPC	--	--	--	--	47±7.2
3a (R110)	Cl	H	H		15±0.8
3b	Br	H	H		7.2±0.6
3c	Cl	H	H		84±10
3d	Cl	H			15±0.7
3e	H	H	H		168±8.2
3f	H	H	H		13±0.8
3g	Cl	H	H		>100
3h	Cl	H	H		36±2.7
3i	3-CF ₃	H	CH ₃		2.6±0.2
3j	3-CF ₃	H	CH ₃		4.2±0.3
3k	3-CF ₃	H	CH ₃		7.9±0.4
4a	H		H		41±2.3
4b	H		H		39±1.0
4c	H		H		28±1.3

^a# (n = 3, values are shown as IC₅₀ ± SD).

Table 3. Potency of MIF2 Tautomerase Inhibition by Thieno[2,3-*d*]pyrimidine-2,4(1*H*,3*H*)-diones Determined Using MIF2-Catalyzed PP Conversion Assay^a

	R ¹	R ²	R ³	IC ₅₀ (μM) [#]
5a	H	Ph		16±0.6
5b	H			15±1.0
7a	CH ₃	Ph	Ph	>100
7b	CH ₃	Ph		7.6±0.5
7c	CH ₃		Ph	19±1.0
7d	CH ₃			5.1±0.5
7e	CH ₃			4.8±0.2
11a	Ph	H		36±3.1
11b		H		27±6.1
7f	CH ₃			1.9±0.1
7g	CH ₃			3.5±0.3
7h	CH ₃			1.7±0.1
7i	CH ₃			4.6±0.3
5c	CH ₃			0.81±0.1
5d	CH ₃			1.0±0.2
5e	CH ₃			2.5±0.2

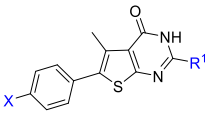
^a# ($n = 3$, values are shown as IC₅₀ ± SD).

its melting temperature in a dose-dependent manner over the DMSO control (Figure 6A). The melting temperature of MIF2 increases by 8.5 °C in the presence of 50 μM **5d**, indicating a binding between **5d** and MIF2. Subsequently, **5d** was subjected to enzyme kinetic analysis for MIF2 inhibition. The Lineweaver–Burk plot shows that the V_{\max} is unaffected by **5d**, while K_M increases with the increase of **5d** concentration (Figure 6B), indicating that **5d** binds in competition with the tautomerase substrate to the active site.

Moreover, we also interrogated the selectivity of **5d** toward MIF2 tautomerase activity by testing its inhibitory potential for MIF tautomerase activity. **5d** provided less than 50% inhibition of MIF tautomerase activity at 50 μM, which indicates a more than 50-fold difference in potency (Figure 6C). Taken together, **5d** is a potent, competitive, and selective binder of MIF2.

Molecular Modeling of the Interaction between 5d and MIF2. To gain insight into the structure–activity

Table 4. Potency of MIF2 Tautomerase Inhibition by Thieno[2,3-*d*]pyrimidin-4(1*H*)-ones Determined Using MIF2-Catalyzed PP Conversion Assay^a



X	R ¹	IC ₅₀ (μM) [#]
8a	Cl	17±1.4
8b	Ph	15±1.4
8c	Ph	17±1.3
8d	OMe	4.3±0.4

^a# (*n* = 3, values are shown as IC₅₀ ± SD).

relationships, a modeling study was done for the binding of inhibitor **5d** to MIF2. **5d** was docked into the tautomerase active site of the crystal structure of MIF2 (PDB code: 6c5f),³² and energy was minimized (Figure 7). The five highest-scoring poses of **5d** occupy similar positions. In this model, the π - π stacking between Phe2 and the phenyl group of R110 (**3a**) is preserved for **5d**. Furthermore, **5d** and Ser50 interact through a hydrogen bond, which is also found between R110 (**3a**) and Lys109. Instead, **5d** has two π -cation interactions with Lys109. Additionally, the CF₃ group of **5d** has several interactions with MIF2 via Phe2, Arg98, and Leu102. Besides, Pro1 and Leu117 are two newly involved interactive residues that can contribute to **5d**-MIF2 binding. These newly formed interactions could explain the increased potency of **5d** compared with R110 (**3a**). Taken together, the putative binding mode rationalizes the binding of **5d** to MIF2 and also sheds light on the increased binding affinity of **5d**.

Antiproliferative Activity of 5d. After the identification of **5d** as a potent MIF2 tautomerase inhibitor, we tested its effect on the proliferation of non-small cell lung cancer (NSCLC) cells. First, we investigated the toxicity of **5d** using a cell viability assay (MTS assay). The results (Figure S4) indicated that **5d** did not show cell viability inhibition up to a concentration of 10 μM in A549, H1650, H1299, and HCC827 cells upon 24 h of exposure. To evaluate the antiproliferative effects of inhibitor **5d**, we treated the cells with **5d** in different concentrations for 72 h before quantifying cell numbers by measuring the DNA content using a CyQUANT

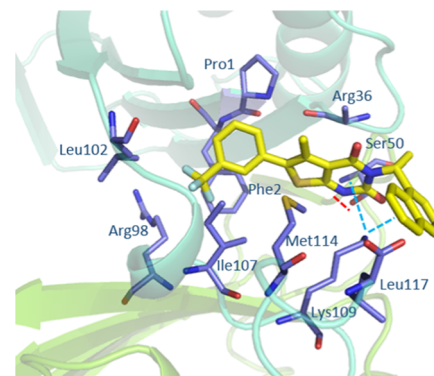


Figure 7. Schematic representation of the binding mode of **5d** (thick sticks) with MIF2 (PDB code: 6c5f).³² The residues of the binding pocket are shown as thin sticks. The hydrogen bond formed with Ser50 is shown as the red dashed line. The cation- π interactions formed with Lys109 are shown as the blue dash line. Discovery Studio was employed for docking and PyMOL was used for graph preparation.

assay. The results indicate that **5d** inhibited the growth of several types of NSCLC cell lines dose-dependently (Figure 8).

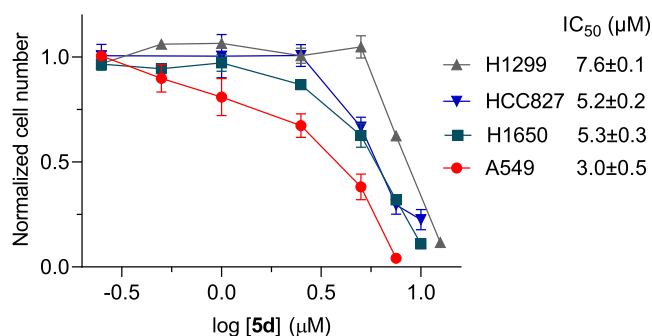


Figure 8. Effect of inhibitor **5d** on the proliferation of the NSCLC cells lines A549, H1650, H1299, and HCC827. The cells were seeded at a density of about 1000 cells per well in a 96-well plate. After overnight culturing, the cells were treated with various concentrations of **5d** for 72 h. Afterward, relative cell numbers were determined by CyQUANT cell proliferation assays and compared with a DMSO-treated control. The data shown are the average of three experiments with SD (*n* = 3).

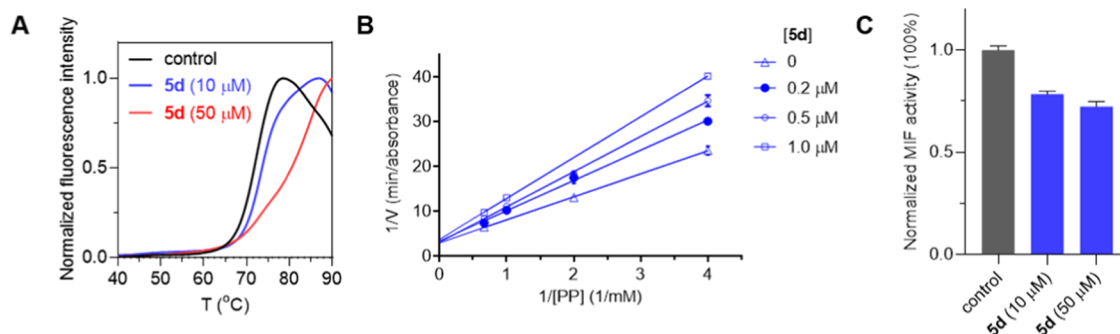


Figure 6. Characterization of **5d**. (A) Fluorescence-based thermal shift assay for the binding of **5d** to MIF2. The melting temperature shows a concentration-dependent shift to a higher temperature in the presence of **5d**. (B) Lineweaver-Burk plot representation. (C) Incubation of MIF with micromolar concentrations of **5d** provided less than 50% inhibition compared to the vehicle control. The data shown are the average of triplicate samples with SD. (*n* = 3, **p* < 0.05, ***p* < 0.01 and ****p* < 0.001 vs control).

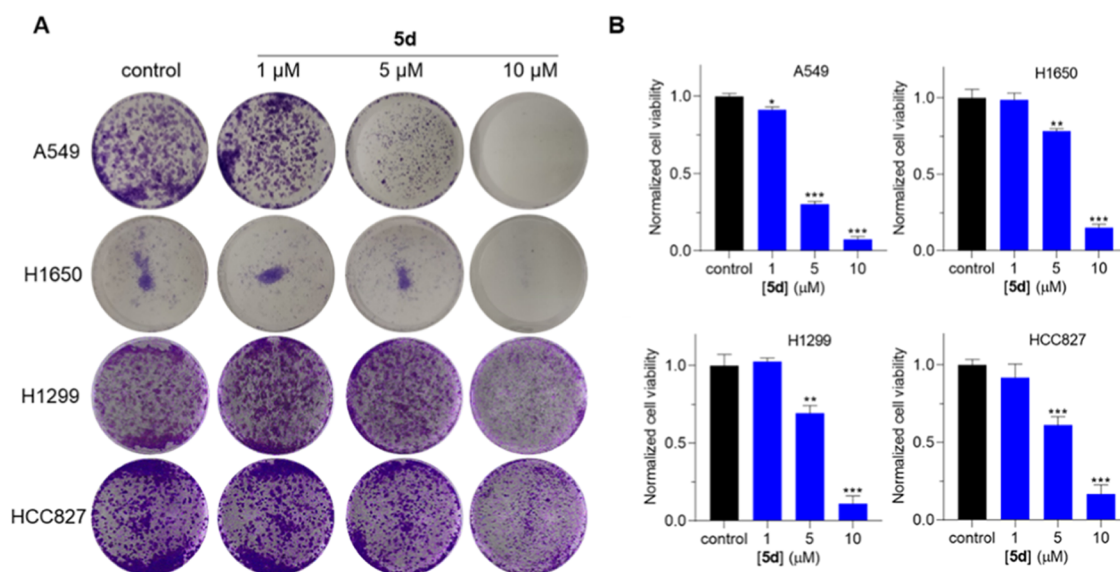


Figure 9. Treatment with inhibitor **5d** inhibits colony formation of NSCLC cell lines. (A) A549 or other NSCLC cell lines were seeded in a 12-well plate (1000 cells/well). The cells were preincubated overnight and were then treated with compounds or vehicle (DMSO) for 5 days. Afterward, the cells were fixed and stained with 0.5% crystal violet solution. Image of representative wells were scanned and are shown. (B) Stained colonies were dissolved in 30% acetic acid and then quantified by measuring the absorbance at 590 nm. The relative colony number is normalized to the DMSO-treated control. The data shown are the average of three experiments with SD ($n = 3$, * $p < 0.05$, ** $p < 0.01$ and *** $p < 0.001$ vs control).

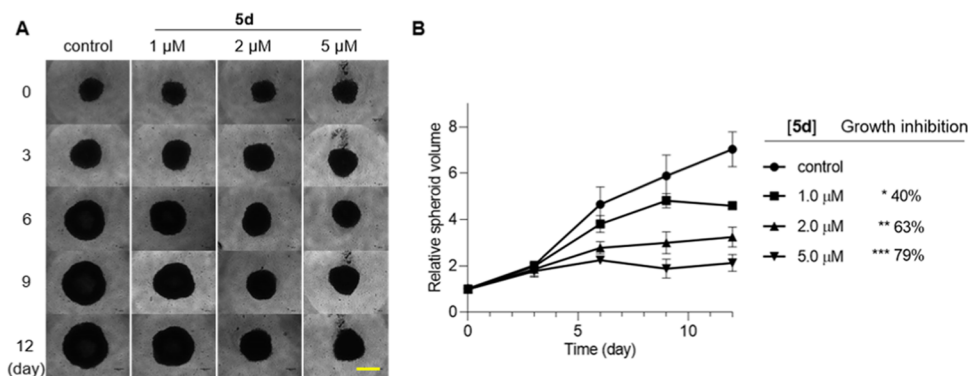


Figure 10. **5d** treatment reduces the growth of A549 cancer cells in a spheroid model. A549 cells were seeded in ultralow attachment 96-well U bottom plate (1000 cells/well) to generate tumor spheroids (a single spheroid per well). After initiation, the spheroids were treated with **5d** at the indicated concentrations every 3 days. DMSO was used as a vehicle control. The day of the first treatment was indicated as day 0. (A) Representative images were obtained at the indicated intervals using an inverted microscope. Scale bar: 500 μm. (B) Analysis was carried out using NIS-Elements AR 3.1 software, and growth curves were obtained relative to the volume of untreated spheroids (day 0) and plotted with GraphPad Prism8. Values are displayed as mean \pm SD ($n = 3$ spheroids for each time point, * $p < 0.05$, ** $p < 0.01$ and *** $p < 0.001$ vs control).

5d showed a visible inhibitory effect at 1 μM and reached about 90% inhibition of cell growth at 7.5 μM on A549 cells, showing an IC_{50} of 3.0 μM. **5d** also inhibited the proliferation of H1650, H1299, and HCC827 cells with IC_{50} values of 5.3, 7.6, and 5.2 μM, respectively. Taken together, these results demonstrate that **5d** inhibits the proliferation of several types of NSCLC cell lines.

The inhibitory effect of **5d** on the proliferation of NSCLC cell lines was further evaluated using a clonogenic assay. The results of this colony formation assay showed that **5d** potently inhibited cell growth of the four NSCLC cell lines tested. We observed a dose-dependent reduction in both colony number and size in **5d**-treated cells compared to vehicle-treated controls (Figure 9A). The number of colonies in each well was quantified by the absorption of crystal violet. **5d** suppressed colony formation in a dose-dependent manner by around 90% in all four NSCLC cell lines tested at a

concentration of 10 μM (Figure 9B). These results confirm the efficacy of **5d** on inhibition of NSCLC cell proliferation.

To gain insights into the effect of longer-term **5d** treatment in a more elaborate model, we employed a 3D spheroid tumor growth model, which was established using A549 cancer cells,³⁹ with each spheroid containing about 1000 A549 cells. After 5-day culturing, different concentrations of **5d** were used to treat these spheroids with 72 h intervals over 12 days. The diameters of spheroid were monitored and compared to day 0 of the treatment. Treatment of **5d** significantly reduced the size of tumor spheroids (Figure 10). With exposure to 1, 2, and 5 μM concentrations of **5d** for 12 days, the volume of spheroid was reduced by 40, 63, and 79%, respectively. These results indicate that the MIF2 tautomerase inhibitor **5d** effectively reduces the growth of A549 cancer cells in a 3D tumor model.

5d Arrests the Cell Cycle of A549 Cells at the G_0/G_1 Phase. The cell cycle progression of **5d**-treated cancer cells

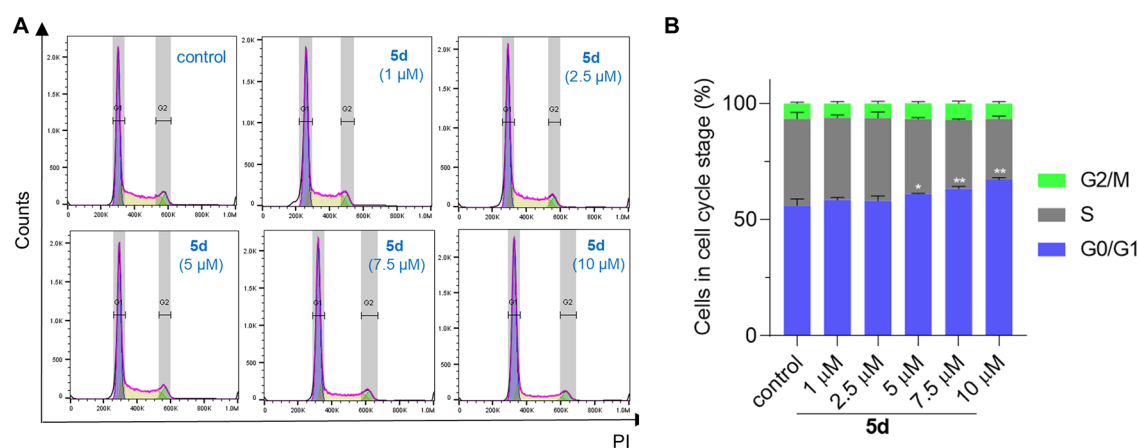


Figure 11. Treatment with **5d** induces cell cycle arrest in A549 cells. (A) A549 cells were treated with **5d** at the indicated concentrations for 48 h. Representative cell cycle distributions graphs obtained using propidium iodide staining-based flow cytometry. (B) Bar graph representatives of the distribution of cells in each phase of the cell cycle (G_0/G_1 , S, and G_2/M phases) were analyzed using FlowJo. Results are displayed as mean \pm SD ($n = 3$, t -test analysis was performed between G_2/M phase of treated groups and control group. * $p < 0.05$ and ** $p < 0.01$ vs control.).

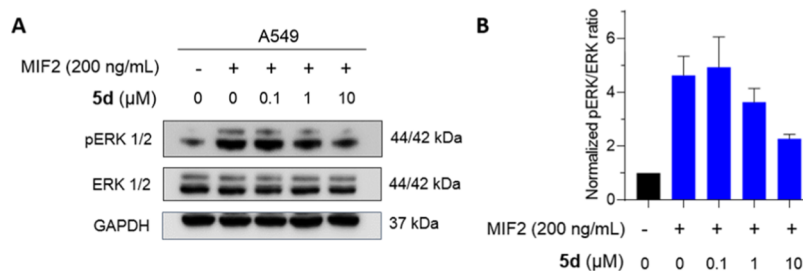


Figure 12. Inhibition of MIF2-induced ERK phosphorylation in A549 cells upon treatment with **5d**. (A) A549 cells were stimulated with recombinant MIF2 with or without **5d** preincubation at indicated concentrations for 15 min; the concentrations of pERK and total ERK were examined by immunoblots with anti-pERK, anti-ERK using glyceraldehyde 3-phosphate dehydrogenase (GAPDH) as a loading control. A representative western blot is shown ($n = 2$). (B) Relative pERK level was quantified by calculating the pERK:ERK ratio and normalized to the control group. Data are displayed as the mean of two experiments.

was investigated using flow cytometry. A549 cells were exposed to different concentrations of **5d** for a duration of 2 days before analysis. The data show that **5d** induced cell cycle arrest at the G_0/G_1 phase dose-dependently (Figure 11). The percentage of A549 cells in the G_0/G_1 phases was 56% for the control group. Upon treatment with 5, 7.5, and 10 μ M **5d**, this percentage increased to 58, 63, and 67%, respectively. This result indicates that **5d** inhibited cell cycle progression, which provided an explanation for the observed inhibition of cancer cell growth.

5d Inhibits ERK Phosphorylation. The effect of **5d** treatment on MIF2-related signaling pathways was studied by assessing MIF2-induced ERK phosphorylation. Towards this aim, MIF2 or **5d** preincubated MIF2 was employed to stimulate A549 cells for 15 min; subsequently, ERK phosphorylation of treated cells was analyzed using western blot detection. MIF2 treatment stimulated ERK phosphorylation in A549 cells to about 4.5-fold of the control. Treatment with **5d** attenuated this stimulation in a dose-dependent manner (Figure 12). These data demonstrate that **5d** treatment inhibits ERK phosphorylation in response to MIF2-stimulation.

DISCUSSION AND CONCLUSIONS

The overexpression of MIF family proteins, MIF and MIF2, has been implicated in several types of cancer.^{40,41} Therefore, MIF and MIF2 are promising drug targets for cancer treatment. A significant effort has been invested into the

development of inhibitory strategies to target MIF.⁴² Nevertheless, the drug discovery efforts to target MIF2 are lagging behind. Thus, the aim of this study was to develop potent small-molecule MIF2 inhibitors that could be applied in cancer therapy.

To discover a potent small-molecule inhibitor to target MIF2, we set up a MIF2-targeted drug discovery campaign, which includes library screening, hit optimization, and a relevant cellular model. Toward this aim, we firstly optimized the 4-HPP based enzyme assay. Although MIF2 possesses an enzymatic activity on catalyzing the keto-enol tautomerization of 4-HPP, its catalytic efficiency is much lower than that of MIF.¹⁷ The structural information shows that the differences inside the enzyme active sites of MIF and MIF2 not only contribute to their unique substrate preference but also facilitate the possibility to develop selective inhibitors such as ISO-1, which is a representative MIF inhibitor that does not inhibit MIF2.¹⁹ Therefore, we set up a MIF2-based tautomerization assay using phenylpyruvate as a substrate. This PP-based assay was employed to screen an in-house library, which afforded several compounds with IC_{50} 's in the low micromolar range. **3a** was selected as the hit for further optimization on the basis of its potency and druglike properties.

The putative binding mode of **3a** with MIF2 reveals that the chlorophenyl group of **3a** is embedded in the pocket and the butyl group is exposed to water. There is vacancy around the

chloro and thiophene groups, as well as a water-exposed rim. To exploit the unoccupied space in the binding site, a focused collection of thiophenes was designed and prepared and MIF2 binding was assessed using a PP-tautomerization assay. We observed that the potency of **3a** analogues can be tuned by different substituents in the thiophene 3-position, and a (naphthalen-1-yl)methyl group proved to be the favorable modification in this series of derivatives. Ring closure of the respective 2-aminothiophene precursor afforded the corresponding thienopyrimidione **5c**, which shows an IC_{50} of 0.81 μM . Thus, inhibitor **5c** gained 50-fold in potency compared to the previously identified MIF2 inhibitor 4-CPPC that proved to have an IC_{50} of 47 μM in our assay format.³⁰ To improve the solubility of **5c**, we disrupted the planarity of **5c** by introducing a methyl group to provide **5d**,³⁸ which has improved solubility and preserved MIF2 binding potency. Notably, **5d** exhibits weak inhibition on MIF thus demonstrating a more than 50-fold selectivity for MIF2 compared to MIF. Taken together, we obtained **5d** as a selective MIF2 tautomerase inhibitor with submicromolar potency and optimal solubility, which enable its use in cellular model systems.

The effect of **5d** on proliferation was evaluated using cell culture assays on several NSCLC cell lines including A549, H1299, HCC827, and H1299. **5d** showed more than 80% inhibition of the proliferation of all four types of tested cancer cells at 10 μM in both a DNA content-based assay and a clonogenic assay. The effectiveness of **5d** was also confirmed on a spheroid cell culture assay, which is able to mimic some of the main features of solid human tumors, such as their cellular layered assembly, hypoxia state, structural organization, and nutrient gradients.⁴³ In this assay, the spheroid volume growth was reduced by 63% upon treatment with 2 μM **5d**. The data demonstrate that **5d** treatment provides a strong inhibition of cell proliferation, which is in line with the previously reported antiproliferation effect of siRNA-mediated MIF2 silencing.^{41,44} We also noticed, compared with our previous studies on MIF tautomerase inhibitors,^{15,35} inhibition of MIF2 tautomerase activity in this study yielded a more substantial impact on cancer cell proliferation. This observation is in line with previous results that MIF2-silencing siRNA inhibited cell growth more potently than MIF-silencing siRNA.⁴¹ Taken together, our results indicate that MIF2 inhibitor **5d** inhibits the cell proliferation of several model systems, which is in line with previous siRNA-based studies on similar model systems.^{41,44}

A main feature of the growth of cancer cells is their continuous and ordered progression of the cell cycle.⁴⁵ Treatment of A549 cancer cells with **5d** arrested cells in the G_0/G_1 phase, indicating interference of cell cycle progression. MIF2 is a growth factor that is involved in the modulation of cell cycle progression through the MAPK pathway.^{41,46} We also observed that **5d** treatment attenuates the MAPK signaling as we found less MIF2-induced ERK phosphorylation. The **5d**-mediated MAPK pathway deactivation is also in line with the effect of siRNA-mediated downregulation of MIF2 protein levels.⁴¹ It is also consistent with the inhibition of ERK phosphorylation by MIF2 inhibitor 4-CPPC.³⁰ Collectively, these data show that the growth inhibition of cancer cell proliferation by **5d** treatment can be explained by ERK phosphorylation blockade and cell cycle progression arrest.

In conclusion, screening of focused compound collections and structure-guided hit optimization enabled the discovery of the potent MIF2 inhibitor **5d**. This inhibitor has submicromolar potency toward MIF2 tautomerase activity, whereas MIF tautomerase activity is not affected. **5d** binds in competition with the MIF2 tautomerase substrate, and its binding was verified by the thermal shift assay in which **5d** improves the MIF2 thermal stability. Furthermore, we have demonstrated that **5d**-mediated inhibition of MIF2 activity suppresses the growth of NSCLC cells in 2D and 3D cell cultures, which can be explained by the inhibition of the MAPK signaling and subsequent cell cycle arrest, thus validating MIF2 as a target with therapeutic potential for NSCLC patients. Taken together, the thienopyrimidione reported here represents a novel molecule for the inhibition of MIF2 with a clear potential for use in cellular model systems.

EXPERIMENTAL SECTION

General. All of the chemicals and solvents were purchased from Sigma-Aldrich, AK Scientific, Fluorochem, or Acros Organics and were used without further processing unless stated otherwise. Thin-layer chromatography (TLC) of Merck silica gel 60 F₂₅₄ plates was used for reaction monitoring. Column chromatography was conducted using MP Ecochrom silica 32–63 (60 Å). ¹H NMR (500 MHz) and ¹³C NMR (126 MHz) were recorded on a Bruker Avance 500 spectrometer. ¹H and ¹³C NMR spectra were reported in parts per million (ppm) referenced to deuterated solvents, for example, CDCl₃: δ = 7.26 ppm (¹H) and 77.05 ppm (¹³C) or DMSO-*d*₆: δ = 2.50 ppm (¹H) and 39.52 ppm (¹³C). To report spin multiplicity, the following abbreviations were used: s (singlet), d (doublet), dd (doublet of doublets), t (triplet), q (quartet), and m (multiplet). Coupling constants were reported in hertz (Hz). Fourier transform mass spectrometry (FTMS) and electrospray ionization (ESI) on an Applied Biosystems/SCIEX API3000-triple quadrupole mass spectrometer were applied for high-resolution mass spectra. Purity of the compounds was confirmed to be >95% by C18 HPLC analysis. The analogues of 4-HPP were synthesized by following a published method.⁴⁷

2-Amino-N-butyl-5-(4-chlorophenyl)thiophene-3-carboxamide (3a). The starting materials **1a–e** and **2a–j** were either purchased or prepared using our previously published methods.⁴⁸ To synthesize **R110 (3a)**, 2-(4-chlorophenyl)acetaldehyde (**1a**, 0.32 g, 2.0 mmol) in EtOH (5 mL) was added into a solution of *N*-butyl-2-cyanoacetamide (**2a**, 0.31 g, 2.1 mmol). To the resulting suspension, triethylamine (0.30 mL, 2.1 mmol) was added, followed by the addition of **S₈** (80 mg, 0.60 mmol). Then, the reaction mixture was refluxed overnight. After cooled down to room temperature, the mixture was diluted using EtOAc (50 mL) and washed with water (2 × 30 mL) and brine (2 × 30 mL). The EtOAc layer was collected and dried over MgSO₄. After filtration, the solvent was collected and removed under reduced pressure and purification was conducted using flash chromatography, with petroleum ether/EtOAc 5:1 (v/v) as eluent. The product (260 mg) was obtained as a light brown solid, yield 42%. ¹H NMR (500 MHz, DMSO-*d*₆) δ 7.70 (t, *J* = 5.6 Hz, 1H), 7.64 (s, 1H), 7.50 (s, 2H), 7.43–7.35 (m, 4H), 3.18 (q, *J* = 6.9 Hz, 2H), 1.47 (p, *J* = 7.3 Hz, 2H), 1.35–1.29 (m, 2H), 0.90 (t, *J* = 7.3 Hz, 3H). ¹³C NMR (126 MHz, DMSO-*d*₆) δ 165.15, 161.12, 133.28, 129.92, 128.94, 125.09, 121.76, 119.86, 108.33, 38.04, 31.58, 19.71, 13.80. HRMS, calculated for C₁₅H₁₈ON₂ClS [M + H]⁺: 309.0823, found 309.0824.

2-Amino-5-(4-bromophenyl)-N-butylthiophene-3-carboxamide (3b).⁴⁸ 2-(4-Bromophenyl)acetaldehyde (0.20 g, 1.0 mmol) and *N*-butyl-2-cyanoacetamide (140 mg, 1.0 mmol) were used to prepare **3b** following the procedure for the synthesis of **3a**, affording compound **3b** (97 mg, yield 28%) as a light yellowish powder. ¹H NMR (500 MHz, DMSO-*d*₆) δ 7.71 (t, *J* = 5.6 Hz, 1H), 7.66 (s, 1H), 7.53 (d, *J* = 8.6 Hz, 2H), 7.32 (d, *J* = 8.6 Hz, 2H), 3.18 (q, *J* = 6.9 Hz, 2H), 1.47 (m, 2H), 1.31 (m, 2H), 0.90 (t, *J* = 7.3 Hz, 3H). ¹³C NMR (126

MHz, DMSO- d_6) δ 165.6, 161.6, 134.1, 132.3, 125.8, 122.3, 120.3, 118.7, 108.8, 38.5, 32.0, 20.2, 14.2. HRMS, calculated for $C_{15}H_{18}ON_2BrS$ [M + H]⁺: 353.0318, found 353.0318.

2-Amino-5-(4-chlorophenyl)-N-phenethylthiophene-3-carboxamide (3c). 2-(4-Chlorophenyl)acetaldehyde (**1a**, 77 mg, 0.50 mmol) and 2-cyano-N-phenethylacetamide (**2b**, 94 mg, 0.50 mmol) were reacted using a procedure similar to the synthesis of **3a**, affording compound **3c** (33 mg, yield 18%) as a light yellowish powder. ¹H NMR (500 MHz, DMSO- d_6) δ 7.88 (t, J = 5.4 Hz, 1H), 7.62 (s, 1H), 7.52 (s, 2H), 7.41 (d, J = 8.6 Hz, 2H), 7.37 (d, J = 8.7 Hz, 2H), 7.30 (t, J = 7.3 Hz, 2H), 7.22 (dd, J = 16.7, 7.0 Hz, 3H), 3.43–3.38 (m, 2H), 2.81 (t, J = 7.5 Hz, 2H). ¹³C NMR (126 MHz, DMSO- d_6) δ 165.20, 161.29, 139.65, 133.24, 129.95, 129.00, 128.93, 128.64, 128.39, 126.09, 125.06, 119.90, 108.21, 40.23, 35.55. MS (ESI): m/z 357.15 [M + H]⁺.

2-Amino-5-phenyl-N-((tetrahydrofuran-3-yl)methyl)thiophene-3-carboxamide (3e). 2-Phenylacetaldehyde (**1d**, 60 mg, 0.50 mmol) and 2-cyano-N-((tetrahydrofuran-3-yl)methyl)acetamide (**2c**, 84 mg, 0.50 mmol) were reacted using a procedure similar to the synthesis of **3a**, affording compound **3e** (52 mg, yield 35%) as a light yellowish powder. ¹H NMR (500 MHz, DMSO- d_6) δ 7.82 (t, J = 5.8 Hz, 1H), 7.67 (s, 1H), 7.46 (s, 2H), 7.40 (d, J = 8.0 Hz, 2H), 7.34 (t, J = 7.8 Hz, 2H), 7.16 (t, J = 7.3 Hz, 1H), 3.93 (p, J = 6.3 Hz, 1H), 3.77 (q, J = 7.1, 6.2 Hz, 1H), 3.62 (q, J = 7.4 Hz, 1H), 3.25 (t, J = 5.9 Hz, 2H), 1.91–1.77 (m, 3H), 1.62–1.52 (m, 1H). ¹³C NMR (126 MHz, DMSO- d_6) δ 165.38, 161.03, 134.30, 128.98, 125.84, 123.58, 121.37, 120.97, 108.01, 77.35, 67.20, 42.59, 28.66, 25.15. HRMS, calculated for $C_{16}H_{19}O_2N_2S$ [M + H]⁺: 303.1162, found 303.1162.

2-Amino-N-octyl-5-phenylthiophene-3-carboxamide (3f). 2-Phenylacetaldehyde (**1d**, 60 mg, 0.50 mmol) and 2-cyano-N-octylacetamide (**2d**, 0.10 g, 0.50 mmol) were reacted using a procedure similar to the synthesis of **3a**, affording compound **3f** (72 mg, yield 44%) as a light yellowish powder. ¹H NMR (500 MHz, DMSO- d_6) δ 7.71 (t, J = 5.6 Hz, 1H), 7.60 (s, 1H), 7.43 (s, 2H), 7.39 (d, J = 7.3 Hz, 2H), 7.34 (t, J = 7.7 Hz, 2H), 7.16 (t, J = 7.7 Hz, 1H), 3.17 (q, J = 6.7 Hz, 2H), 1.52–1.43 (m, 2H), 1.30–1.23 (m, 10H), 0.85 (t, J = 6.8 Hz, 3H). ¹³C NMR (126 MHz, DMSO- d_6) δ 165.23, 160.77, 134.30, 128.98, 125.83, 123.63, 121.35, 120.67, 108.25, 38.40, 31.32, 29.47, 28.86, 28.74, 26.60, 22.15, 14.00. HRMS, calculated for $C_{19}H_{27}N_2S$ [M + H]⁺: 331.1839, found 331.1839.

2-Amino-5-(4-chlorophenyl)-N-(2-ethoxyethyl)thiophene-3-carboxamide (3g). 2-(4-Chlorophenyl)acetaldehyde (**1a**, 77 mg, 0.50 mmol) and 2-cyano-N-(2-ethoxyethyl)acetamide (**2e**, 80 mg, 0.50 mmol) were reacted using a procedure similar to the synthesis of **3a**, affording compound **3g** (88 mg, yield 56%) as a light yellowish powder. ¹H NMR (500 MHz, CDCl₃) δ 7.34 (d, J = 8.6 Hz, 2H), 7.29 (d, J = 8.6 Hz, 2H), 6.94 (s, 1H), 6.23 (s, 2H), 6.11 (s, 1H), 3.58 (d, J = 2.5 Hz, 4H), 3.55 (q, J = 7.0 Hz, 2H), 1.24 (t, J = 7.0 Hz, 3H). ¹³C NMR (126 MHz, CDCl₃) δ 165.78, 160.62, 132.68, 132.35, 129.12, 125.94, 123.98, 118.84, 109.92, 69.45, 66.65, 39.20, 15.32. HRMS, calculated for $C_{15}H_{18}ON_2$ CIS [M + H]⁺: 325.0772, found 325.0773.

2-Amino-N-(4-chlorophenethyl)-5-(4-chlorophenyl)thiophene-3-carboxamide (3h). 2-(4-Chlorophenyl)acetaldehyde (**1a**, 77 mg, 0.50 mmol) and N-(4-chlorophenethyl)-2-cyanoacetamide (**2f**, 0.10 g, 0.50 mmol) were reacted using a procedure similar to the synthesis of **3a**, affording compound **3h** (66 mg, yield 34%) as a light yellowish powder. ¹H NMR (500 MHz, DMSO- d_6) δ 7.85 (t, J = 5.6 Hz, 1H), 7.60 (s, 1H), 7.51 (s, 2H), 7.41 (d, J = 8.8 Hz, 2H), 7.37 (d, J = 9.0 Hz, 2H), 7.35 (d, J = 8.4 Hz, 2H), 7.26 (d, J = 8.4 Hz, 2H), 3.40 (q, J = 7.1 Hz, 2H), 2.80 (t, J = 7.3 Hz, 2H). ¹³C NMR (126 MHz, DMSO- d_6) δ 165.22, 161.33, 138.72, 133.22, 130.73, 130.57, 129.97, 129.01, 128.94, 128.28, 125.08, 119.91, 108.13, 40.11, 34.73. MS (ESI): m/z 391.10 [M + H]⁺.

2-Amino-N,4-dibutyl-5-(4-chlorophenyl)thiophene-3-carboxamide (3d). 1-(4-Chlorophenyl)hexan-2-one (**1c**, 0.20 g, 1.0 mmol) and 2-(4-chlorophenyl)acetaldehyde (**1a**, 0.15 g, 1.0 mmol) were dissolved in dry THF (5 mL). To the stirred solution, SnCl₄ (0.22 mL, 2.0 mmol) was added dropwisely. Then, Et₃N (0.30 mL) was added. The reaction mixture was stirred at 40 °C for 16 h, followed by

the addition of HCl solution (1 N, 25 mL) and extraction with EtOAc (3 × 20 mL). The combined organic layers were washed with a NaOH solution (1 N, 25 mL) and dried over MgSO₄. The solid was filtered, and the solvent was removed using evaporation under reduced pressure. The resulting mixture was dissolved in EtOH (5 mL), and S₈ (32 mg, 0.25 mmol) and Et₃N (0.2 mL) were added. The reaction mixture was refluxed overnight. Then, the mixture was diluted with EtOAc (25 mL) and washed with water (2 × 50 mL) and brine (2 × 50 mL). The organic layers were dried over MgSO₄, filtrated, and the solvent was removed using evaporation under reduced pressure. The product was obtained as a brown solid (151 mg, yield 41%) after chromatography using petroleum ether:EtOAc 30:1 (v/v) as eluent. ¹H NMR (500 MHz, DMSO- d_6) δ 7.64 (t, J = 5.6 Hz, 1H), 7.45 (d, J = 8.5 Hz, 2H), 7.28 (d, J = 8.5 Hz, 2H), 6.21 (s, 2H), 3.19 (q, J = 6.8 Hz, 2H), 2.66–2.58 (m, 2H), 1.49–1.43 (m, 2H), 1.33 (dt, J = 14.9, 7.2 Hz, 4H), 1.16 (q, J = 7.3 Hz, 2H), 0.89 (t, J = 7.3 Hz, 3H), 0.76 (t, J = 7.3 Hz, 3H). ¹³C NMR (126 MHz, DMSO- d_6) δ 165.47, 155.55, 135.69, 133.52, 131.11, 130.51, 128.70, 117.17, 113.51, 38.36, 32.22, 31.39, 27.12, 22.10, 19.79, 13.79, 13.65. HRMS, calculated for $C_{19}H_{26}ON_2ClS$ [M + H]⁺: 365.1449, found 365.1449.

2-Amino-4-methyl-N-(naphthalen-1-ylmethyl)-5-(3-(trifluoromethyl)phenyl)thiophene-3-carboxamide (3i). 1-(3-(Trifluoromethyl)phenyl)propan-2-on (**1e**, 0.30 g, 1.5 mmol) and 2-cyano-N-(naphthalen-1-ylmethyl)acetamide (**2h**, 0.30 g, 1.5 mmol) were reacted using a procedure similar to the synthesis of **3d**, affording compound **3i** (178 mg, yield 28%) as a brown solid. ¹H NMR (500 MHz, CDCl₃) δ 8.08 (d, J = 8.3 Hz, 1H), 7.89 (d, J = 8.0 Hz, 1H), 7.83 (d, J = 8.1 Hz, 1H), 7.58–7.42 (m, 8H), 6.10 (s, 1H), 5.07 (d, J = 5.0 Hz, 2H), 2.16 (s, 3H). ¹³C NMR (126 MHz, CDCl₃) δ 166.2, 135.0, 134.1, 133.6, 132.9, 131.5, 131.1, 130.9 (q, J = 32.2 Hz), 129.1, 129.0, 128.9, 128.8, 126.8, 126.3 (q, J = 3.6 Hz), 126.2, 126.1 (q, J = 234.9 Hz), 125.7, 125.6, 123.7 (q, J = 3.7 Hz), 123.5, 119.8, 112.1, 42.0, 16.2. HRMS, calculated for $C_{24}H_{20}ON_2F_3S$ [M + H]⁺: 441.1243, found 441.1240.

(R)-2-Amino-4-methyl-N-(1-(naphthalen-1-yl)ethyl)-5-(3-(trifluoromethyl)phenyl)thiophene-3-carboxamide (3j). 1-(3-(Trifluoromethyl)phenyl)propan-2-on (**1e**, 0.41 g, 2.0 mmol) and (R)-2-cyano-N-(1-(naphthalen-1-yl)ethyl)acetamide (**2i**, 0.50 g, 2.0 mmol) were reacted using a procedure similar to the synthesis of **3d**, affording compound **3j** (146 mg, yield 16%) as a brown solid. ¹H NMR (500 MHz, CDCl₃) δ 8.18 (d, J = 8.5 Hz, 1H), 7.88 (d, J = 8.1 Hz, 1H), 7.81 (d, J = 8.2 Hz, 1H), 7.59–7.43 (m, 8H), 6.19–6.02 (m, 3H), 2.19 (s, 3H), 1.78 (d, J = 5.9 Hz, 3H). ¹³C NMR (126 MHz, CDCl₃) δ 165.4, 138.6, 135.0, 134.2, 132.9, 131.2, 131.1, 130.9 (q, J = 20.7 Hz), 129.1, 129.0, 128.9, 128.5, 127.5 (q, J = 306.1 Hz), 126.7, 126.3, 126.3, 126.0, 125.4, 123.7 (q, J = 4.9 Hz), 123.5, 123.0, 122.7, 45.0, 21.4, 16.2. HRMS, calculated for $C_{25}H_{22}ON_2F_3S$ [M + H]⁺: 455.1399, found 455.1397.

(S)-2-Amino-4-methyl-N-(1-(naphthalen-1-yl)ethyl)-5-(3-(trifluoromethyl)phenyl)thiophene-3-carboxamide (3k). 1-(3-(Trifluoromethyl)phenyl)propan-2-on (**1e**, 0.2 g, 1 mmol) and (S)-2-cyano-N-(1-(naphthalen-1-yl)ethyl)acetamide (**2i**, 0.20 g, 1.0 mmol) were reacted using a procedure similar to the synthesis of **3d**, affording compound **3k** (0.20 g, yield 42%) as a brown solid. ¹H NMR (500 MHz, CDCl₃) δ 8.19 (d, J = 8.5 Hz, 1H), 7.88 (d, J = 8.1 Hz, 1H), 7.82 (d, J = 8.2 Hz, 1H), 7.63–7.39 (m, 9H), 6.13–6.07 (m, 2H), 2.19 (s, 3H), 1.81 (m, 3H). ¹³C NMR (126 MHz, CDCl₃) δ 165.4, 138.6, 135.0, 134.2, 132.9, 131.1, 130.9, 129.1, 129.1, 128.9, 128.5, 126.7, 126.3, 126.3, 126.0, 125.5 (q, J = 285.6 Hz), 125.4, 123.9, 123.7, 123.5, 123.0, 122.7, 45.1, 21.4, 16.2. HRMS, calculated for $C_{25}H_{22}ON_2F_3S$ [M + H]⁺: 455.1399, found 455.1398.

2-Acetamido-N-butyl-5-phenylthiophene-3-carboxamide (4a). To a stirred solution of 2-amino-N-butyl-5-phenylthiophene-3-carboxamide (0.30 g, 1.0 mmol) in DMF (4 mL), acyl chloride (2.0 mmol) and pyridine (2 mmol) were added. The reaction mixture was stirred at room temperature overnight. Subsequently, the reaction mixture was diluted with CH₂Cl₂ (20 mL) and was sequentially washed with HCl (1 N, 20 mL), saturated NaHCO₃ (20 mL), water (20 mL), and brine (2 × 20 mL). The organic layer was collected and

dried over MgSO_4 . After filtration, the solvent was removed under reduced pressure. The product was obtained as a brown solid (182 mg, yield 58%). ^1H NMR (500 MHz, $\text{DMSO}-d_6$) δ 12.06 (s, 1H), 8.39 (t, $J = 5.5$ Hz, 1H), 7.88 (s, 1H), 7.57 (d, $J = 7.3$ Hz, 2H), 7.42 (t, $J = 7.8$ Hz, 2H), 7.29 (t, $J = 7.9$ Hz, 1H), 3.28 (q, $J = 7.0$ Hz, 2H), 2.22 (s, 3H), 1.53 (p, $J = 7.4$ Hz, 2H), 1.34 (h, $J = 7.3$ Hz, 2H), 0.91 (t, $J = 7.4$ Hz, 3H). ^{13}C NMR (126 MHz, $\text{DMSO}-d_6$) δ 166.99, 164.51, 144.58, 133.62, 131.67, 129.31, 127.31, 124.82, 118.78, 115.85, 38.45, 31.23, 23.22, 19.71, 13.75. HRMS, calculated for $\text{C}_{17}\text{H}_{21}\text{O}_2\text{N}_2\text{S}$ [$\text{M} + \text{H}$] $^+$: 317.1318, found 317.1317.

N-Butyl-2-butylamido-5-phenylthiophene-3-carboxamide (4b). **4b** was prepared by following the similar procedure for the synthesis of **4a**. Product was obtained as a brown solid (152 mg, yield 44%). ^1H NMR (500 MHz, $\text{DMSO}-d_6$) δ 12.2 (s, 1H), 8.4 (t, $J = 5.7$ Hz, 1H), 7.9 (s, 1H), 7.6–7.5 (m, 2H), 7.4 (t, $J = 7.7$ Hz, 2H), 7.3 (td, $J = 7.3, 1.1$ Hz, 1H), 3.3 (td, $J = 7.1, 5.6$ Hz, 2H), 2.5 (t, $J = 7.3$ Hz, 2H), 1.6 (h, $J = 7.3$ Hz, 2H), 1.5 (tt, $J = 7.7, 6.5$ Hz, 2H), 1.3 (h, $J = 7.3$ Hz, 2H), 0.9 (dt, $J = 10.0, 7.3$ Hz, 6H) ppm. ^{13}C NMR (126 MHz, $\text{DMSO}-d_6$) δ 169.6, 164.6, 144.6, 133.6, 131.7, 129.2, 127.3, 124.8, 124.6, 118.8, 118.6, 115.9, 38.5, 37.6, 31.2, 19.7, 18.3, 13.7, 13.5. HRMS, calculated for $\text{C}_{19}\text{H}_{25}\text{O}_2\text{N}_2\text{S}$ [$\text{M} + \text{H}$] $^+$: 345.1631, found 345.1631.

N-Butyl-2-heptanamido-5-phenylthiophene-3-carboxamide (4c). **4c** was prepared by following the similar procedure for the synthesis of **4a**. Product was obtained as a brown solid (195 mg, yield 51%). ^1H NMR (500 MHz, $\text{DMSO}-d_6$) δ 12.15 (s, 1H), 8.39 (t, $J = 5.6$ Hz, 1H), 7.88 (s, 1H), 7.57 (d, $J = 7.5$ Hz, 2H), 7.43 (t, $J = 7.8$ Hz, 2H), 7.29 (t, $J = 7.4$ Hz, 1H), 2.49–2.45 (m, 2H), 2.18 (t, $J = 7.4$ Hz, 2H), 1.61 (p, $J = 7.2$ Hz, 2H), 1.53 (p, $J = 7.4$ Hz, 2H), 1.35 (dt, $J = 14.8, 7.4$ Hz, 2H), 1.27–1.23 (m, 8H), 0.91 (t, $J = 7.4$ Hz, 3H), 0.85 (s, 3H). ^{13}C NMR (126 MHz, $\text{DMSO}-d_6$) δ 174.98, 170.15, 165.03, 145.02, 134.09, 132.11, 129.67, 127.74, 125.06, 116.31, 38.90, 36.15, 34.12, 31.62, 28.94, 25.23, 24.97, 22.53, 20.15, 14.42, 14.19. HRMS, calculated for $\text{C}_{23}\text{H}_{33}\text{O}_2\text{N}_2\text{S}$ [$\text{M} + \text{H}$] $^+$: 401.2255, found 401.2254.

3-Butyl-6-phenylthieno[2,3-d]pyrimidine-2,4(1H,3H)-dione (5a). **5a**. To a solution of 2-amino-N-butyl-5-phenylthiophene-3-carboxamide (0.3 g, 1.0 mmol) in DCM (10 mL), 1,1-carbonyldiimidazole (CDI, 0.50 g, 3.1 mmol) was added, and the solution was refluxed for 16 h. Subsequently, the solvent was removed under reduced pressure and EtOAc (25 mL) was added to dissolve the residual mixture. The organic solution was then washed with water (25 mL) and brine (25 mL). The EtOAc layer was collected and dried over MgSO_4 . After the removal of MgSO_4 by filtration, the solvent was removed using evaporation under reduced pressure. The purification was done using chromatography with petroleum ether:EtOAc 3:1 (v/v) as an eluent, and a 159 mg light yellow solid was obtained as the product. Yield 52%. ^1H NMR (500 MHz, $\text{DMSO}-d_6$) δ 7.66 (d, $J = 7.4$ Hz, 2H), 7.58 (s, 1H), 7.41 (t, $J = 7.7$ Hz, 2H), 7.32 (t, $J = 7.4$ Hz, 1H), 3.96–3.73 (m, 2H), 1.53 (p, $J = 7.5$ Hz, 2H), 1.30 (h, $J = 7.4$ Hz, 2H), 0.90 (t, $J = 7.4$ Hz, 3H). ^{13}C NMR (126 MHz, $\text{DMSO}-d_6$) δ 158.32, 150.26, 149.70, 133.44, 132.60, 129.25, 127.95, 125.29, 118.10, 115.60, 29.48, 22.39, 19.68, 13.76. HRMS, calculated for $\text{C}_{16}\text{H}_{17}\text{O}_2\text{N}_2$ [$\text{M} + \text{H}$] $^+$: 301.1005, found 301.1006.

3-Allyl-6-(4-chlorophenyl)thieno[2,3-d]pyrimidine-2,4(1H,3H)-dione (5b). **N-Allyl-2-amino-5-(4-chlorophenyl)thiophene-3-carboxamide** (0.30 g, 1.0 mmol) was reacted with CDI (0.50 g, 3.0 mmol) following a similar method for the synthesis of **5a** to provide **5b** as a 126 mg light yellow solid. Yield 40%. ^1H NMR (500 MHz, $\text{DMSO}-d_6$) δ 12.39 (s, 1H), 7.69 (d, $J = 8.4$ Hz, 2H), 7.65 (s, 1H), 7.46 (d, $J = 8.4$ Hz, 2H), 5.85 (dq, $J = 16.0, 5.2$ Hz, 1H), 5.14–5.05 (m, 2H), 4.45 (d, $J = 4.5$ Hz, 2H). ^{13}C NMR (126 MHz, $\text{DMSO}-d_6$) δ 157.93, 150.19, 149.97, 132.71, 132.33, 132.11, 131.53, 129.14, 126.90, 118.89, 116.23, 115.55, 41.93. MS (ESI): m/z 319.08 [$\text{M} + \text{H}$] $^+$.

5-Methyl-3-(naphthalen-1-ylmethyl)-6-(3-(trifluoromethyl)phenyl)thieno[2,3-d]pyrimidine-2,4(1H,3H)-dione (5c). **5c** (50 mg, 0.10 mmol) and CDI (50 mg, 0.31 mmol) were reacted using a procedure similar to the synthesis of **5a**, affording compound **5c** (48 mg, yield 91%) as a brown solid. ^1H NMR (500 MHz, $\text{DMSO}-d_6$) δ 12.56 (s, 1H), 8.22 (d, $J = 8.3$ Hz, 1H), 7.98 (d, $J = 8.0$ Hz, 1H),

7.84–7.72 (m, 5H), 7.64–7.56 (m, 2H), 7.42 (t, $J = 7.7$ Hz, 1H), 7.10 (d, $J = 7.2$ Hz, 1H), 5.53 (s, 2H), 2.44 (s, 3H). ^{13}C NMR (126 MHz, $\text{DMSO}-d_6$) δ 159.3, 151.2, 150.2, 133.5, 133.4 (q, $J = 15.3$ Hz), 133.2, 132.2, 131.2, 130.4, 130.2, 129.9, 129.6, 128.7, 127.2, 127.1, 126.4, 125.8, 125.5, 125.1, 123.8 (q, $J = 231.0$ Hz), 123.0, 122.0, 113.8, 40.9, 14.1. HRMS, calculated for $\text{C}_{25}\text{H}_{18}\text{O}_2\text{N}_2\text{F}_3\text{S}$ [$\text{M} + \text{H}$] $^+$: 467.1036, found 467.1034.

(R)-5-Methyl-3-(1-(naphthalen-1-yl)ethyl)-6-(3-(trifluoromethyl)phenyl)thieno[2,3-d]pyrimidine-2,4(1H,3H)-dione (5d). **5d** (0.10 g, 0.50 mmol) and CDI (0.20 g, 1.2 mmol) were reacted using a procedure similar to the synthesis of **5a**, affording compound **5d** (68 mg, yield 64%) as a brown solid. ^1H NMR (500 MHz, CDCl_3) δ 11.27 (s, 1H), 7.98 (dd, $J = 10.4, 7.9$ Hz, 2H), 7.80 (d, $J = 8.3$ Hz, 1H), 7.76 (d, $J = 8.2$ Hz, 1H), 7.65 (t, $J = 3.6$ Hz, 2H), 7.62–7.57 (m, 2H), 7.53–7.49 (m, 1H), 7.46–7.37 (m, 2H), 6.91 (q, $J = 7.0$ Hz, 1H), 2.56 (s, 3H), 2.03 (d, $J = 7.0$ Hz, 3H). ^{13}C NMR (126 MHz, CDCl_3) δ 159.5, 152.3, 150.0, 134.7, 133.8, 133.7, 132.9, 132.3, 131.8, 131.5 (q, $J = 32.1$ Hz), 129.5, 129.1, 128.4, 127.9, 126.6, 126.4, 126.3 (q, $J = 3.7$ Hz), 126.1 (q, $J = 251.2$ Hz), 125.3, 125.0, 124.8 (q, $J = 3.4$ Hz), 123.2, 115.3, 47.9, 16.9, 14.7. HRMS, calculated for $\text{C}_{26}\text{H}_{20}\text{O}_2\text{N}_2\text{F}_3\text{S}$ [$\text{M} + \text{H}$] $^+$: 481.1192, found 481.1192.

(S)-5-Methyl-3-(1-(naphthalen-1-yl)ethyl)-6-(3-(trifluoromethyl)phenyl)thieno[2,3-d]pyrimidine-2,4(1H,3H)-dione (5e). **5e** (0.10 g, 0.50 mmol) and CDI (0.20 g, 1.2 mmol) were reacted using a procedure similar to the synthesis of **5a**, affording compound **5e** (82 mg, yield 77%) as a light yellow solid. ^1H NMR (500 MHz, CDCl_3) δ 11.13 (s, 1H), 7.97 (m, 2H), 7.81 (d, $J = 7.8$ Hz, 1H), 7.76 (d, $J = 8.2$ Hz, 1H), 7.64 (d, $J = 5.4$ Hz, 2H), 7.59 (d, $J = 3.5$ Hz, 2H), 7.51 (t, $J = 7.7$ Hz, 1H), 7.42 (dt, $J = 22.1, 7.4$ Hz, 2H), 6.91 (q, $J = 6.6$ Hz, 1H), 2.55 (s, 3H), 2.03 (d, $J = 6.9$ Hz, 3H). ^{13}C NMR (126 MHz, CDCl_3) δ 159.5, 152.1, 150.0, 134.8, 133.8, 133.7, 132.9, 132.3, 131.8, 131.5 (q, $J = 32.8$ Hz), 129.5, 129.1, 128.4, 127.9, 126.7, 126.3, 126.0 (q, $J = 236.1$ Hz), 125.4, 125.0, 124.8 (q, $J = 3.4$), 123.2, 115.3, 47.9, 16.9, 14.6. HRMS, calculated for $\text{C}_{26}\text{H}_{20}\text{O}_2\text{N}_2\text{F}_3\text{S}$ [$\text{M} + \text{H}$] $^+$: 481.1192, found 481.1192.

Ethyl 2-Amino-4-methyl-5-phenylthiophene-3-carboxylate (6a). **6a**. A mixture of phenolacetone (**1f**, 0.7 mL, 5 mmol), ethyl cyanoacetate (0.5 mL, 5 mmol), ammonium acetate (0.1 g, 1 mmol), and acetic acid (0.2 mL, 4 mmol) in toluene (5 mL) was heated under reflux for 20 h, while water was removed using a molecular sieve. After the mixture was cooled to room temperature, the mixture was concentrated *in vacuo*. The residue was diluted with saturated NaHCO_3 (20 mL) and extracted with CHCl_3 (3×25 mL). The extract was washed with brine (25 mL) and dried (MgSO_4). After evaporation of the solvent *in vacuo*, the residue was purified by flash column chromatography to give an oil-like intermediate, which was dissolved in EtOH (9 mL). To the solution were added sulfur powder (0.13 g, 4.0 mmol) and triethylamine (0.6 mL, 4 mmol), and the resulting mixture was stirred at 100 °C for 2 h. After removal of the solvent *in vacuo*, the residue was diluted with brine and extracted with CHCl_3 (3×25 mL). The organic layers were collected and washed with brine (25 mL) and dried (MgSO_4). The solution was concentrated *in vacuo*, and the residue was recrystallized from CHCl_3 to afford **6a** (1.1 g, 81%) as dark brown crystals. ^1H NMR (500 MHz, $\text{DMSO}-d_6$) δ 7.82 (t, $J = 5.8$ Hz, 1H), 7.46 (s, 2H), 7.40 (d, $J = 8.0$ Hz, 2H), 7.34 (t, $J = 7.8$ Hz, 2H), 4.36 (q, $J = 7.0$ Hz, 3H), 1.34 (t, $J = 7.1$ Hz, 3H).

Ethyl 2-Amino-5-(4-chlorophenyl)-4-methylthiophene-3-carboxylate (6b). 4-Chlorophenylacetone (**1j**, 0.7 mL, 5 mmol) and ethyl cyanoacetate (0.5 g, 5 mmol) were reacted using a procedure similar to the synthesis of **6a**, affording compound **6b** (0.9 g, yield 61%) as a brown solid. ^1H NMR (500 MHz, CDCl_3) δ 7.34 (d, $J = 8.5$ Hz, 2H), 7.27 (d, $J = 7.3$ Hz, 2H), 6.12 (s, 2H), 4.35–4.28 (m, 2H), 2.30 (s, 3H), 1.37 (t, $J = 7.1$ Hz, 3H).

Ethyl 2-Amino-5-(3,4-dichlorophenyl)-4-methylthiophene-3-carboxylate (6c). 1-(3,4-Dichlorophenyl)propan-2-one (**1k**, 0.3 mL, 2 mmol) and ethyl cyanoacetate (0.5 g, 5 mmol) were reacted using a procedure similar to the synthesis of **6a**, affording compound **6c** (0.3 g, yield 39%) as a brown solid. ^1H NMR (500 MHz, methanol- d_4) δ

7.54 (s, 1H), 7.29 (d, $J = 7.1$ Hz, 1H), 7.27 (d, $J = 7.1$ Hz, 1H), 4.13 (q, $J = 7.0$ Hz, 32), 2.05 (s, 3H), 1.27 (t, $J = 7.1$ Hz, 3H).

Ethyl 2-Amino-5-(2,4-dichlorophenyl)-4-methylthiophene-3-carboxylate (6d). 1-(2,4-Dichlorophenyl)propan-2-one (**1l**, 0.3 mL, 2 mmol) and ethyl cyanoacetate (0.3 g, 3 mmol) were reacted using a procedure similar to the synthesis of **6a**, affording compound **6d** (0.3 g, yield 49%) as a brown solid. ^1H NMR (500 MHz, DMSO- d_6) δ 7.72 (d, $J = 2.1$ Hz, 1H), 7.49–7.38 (m, 4H), 4.20 (q, $J = 7.1$ Hz, 2H), 1.99 (s, 3H), 1.27 (t, $J = 7.1$ Hz, 3H).

Ethyl 2-Amino-4-methyl-5-(3-(trifluoromethyl)phenyl)thiophene-3-carboxylate (6e). **1e** (0.7 mL, 5 mmol) and ethyl cyanoacetate (0.5 g, 5 mmol) were reacted using a procedure similar to the synthesis of **6a**, affording compound **6e** (1.0 g, yield 68%) as a brown solid. ^1H NMR (500 MHz, DMSO- d_6) δ 7.64 (m, 3H), 7.58 (s, 1H), 7.55 (s, 2H), 4.22 (q, $J = 7.1$ Hz, 2H), 2.26 (s, 3H), 1.28 (t, $J = 7.1$ Hz, 3H).

Ethyl 2-Amino-5-(benzo[d][1,3]dioxol-5-yl)-4-methylthiophene-3-carboxylate (6f). 1-(Benzo[d][1,3]dioxol-5-yl)propan-2-one (**1m**, 0.3 mL, 2 mmol) and ethyl cyanoacetate (0.5 g, 5 mmol) were reacted using a procedure similar to the synthesis of **6a**, affording compound **6b** (0.2 g, yield 28%) as a brown solid. ^1H NMR (500 MHz, CDCl $_3$) δ 7.74 (s, 1H), 7.44 (d, $J = 6.8$ Hz, 1H), 6.94 (d, $J = 6.1$ Hz, 1H), 6.84 (s, 2H), 6.12 (s, 2H), 4.39 (q, $J = 6.8$ Hz, 2H), 2.31 (s, 3H), 1.40 (t, $J = 6.5$ Hz, 3H).

Ethyl 2-Amino-5-(4-fluorophenyl)-4-methylthiophene-3-carboxylate (6g). 1-(Benzo[d][1,3]dioxol-5-yl)propan-2-one (**1m**, 0.70 mL, 5.0 mmol) and ethyl cyanoacetate (0.55 g, 5.0 mmol) were reacted using a procedure similar to the synthesis of **6a**, affording compound **6b** (0.81 g, yield 59%) as a brown solid. ^1H NMR (500 MHz, methanol- d_4) δ 7.37–7.31 (m, 2H), 7.14–7.10 (m, 2H), 4.30 (q, $J = 7.1$ Hz, 2H), 2.27 (s, 3H), 1.37 (t, $J = 7.1$ Hz, 3H).

Synthesis of 7a–i. 5-Methyl-3,6-diphenylthieno[2,3-*d*]pyrimidine-2,4(1*H*,3*H*)-dione (7a). To a stirred solution of **6a** (0.3 g, 1 mmol) in pyridine (3 mL), phenyl isocyanate (0.21 mL, 1.5 mmol) was added and stirred at 45 °C for overnight. The resulting mixture was concentrated reduced pressure, and the residue was suspended in MeOH (5 mL). To the suspension, 25% sodium methoxide (0.6 mL, 3 mmol) was added and the resulting mixture was stirred for 6 h at room temperature. Subsequently, the mixture was acidified with 1 N HCl (10 mL) at 0 °C and the pH was regulated to 4. The organic solvent was evaporated to a volume of about 5 mL, and the precipitate was collected. The obtained solid was dissolved in methanol and purified with chromatography using DCM:MeOH (100:1) as a solvent. The product was obtained as light brown crystals (135 mg, yield 40%). ^1H NMR (500 MHz, DMSO- d_6) δ 12.37 (s, 1H), 7.51–7.39 (m, 8H), 7.31–7.27 (m, 2H), 2.40 (s, 3H). ^{13}C NMR (126 MHz, DMSO- d_6) δ 159.44, 150.86, 150.15, 135.79, 132.38, 129.83, 129.22, 129.07, 128.99, 128.86, 128.71, 127.97, 126.74, 114.19, 14.15. HRMS, calculated for C $_{19}$ H $_{15}$ O $_2$ N $_2$ S [M + H] $^+$: 335.0849, found 335.0849.

3-Benzyl-5-methyl-6-phenylthieno[2,3-*d*]pyrimidine-2,4(1*H*,3*H*)-dione (7b). **6a** (0.3 g, 1 mmol) and benzyl isocyanate (0.2 mL, 1.5 mmol) were reacted using a procedure similar to the synthesis of **7a**, affording compound **7b** (150 mg, yield 43%) as a white solid. ^1H NMR (500 MHz, DMSO- d_6) δ 12.36 (s, 1H), 7.49–7.44 (m, 4H), 7.39 (t, $J = 6.8$ Hz, 1H), 7.32–7.30 (m, 4H), 7.25–7.23 (m, 1H), 5.04 (s, 2H), 2.43 (s, 3H). ^{13}C NMR (126 MHz, DMSO- d_6) δ 159.19, 150.43, 150.20, 137.49, 132.34, 129.65, 129.16, 129.08, 128.34, 127.97, 127.40, 127.04, 126.86, 113.76, 42.89, 14.15. HRMS, calculated for C $_{20}$ H $_{17}$ O $_2$ N $_2$ S [M + H] $^+$: 349.1005, found 349.1004.

6-(4-Chlorophenyl)-5-methyl-3-phenylthieno[2,3-*d*]pyrimidine-2,4(1*H*,3*H*)-dione (7c). **6b** (0.3 g, 1 mmol) and phenyl isocyanate (0.2 mL, 1.5 mmol) were reacted using a procedure similar to the synthesis of **7a**, affording compound **7c** (93 mg, yield 31%) as a white solid. ^1H NMR (500 MHz, DMSO- d_6) δ 12.40 (s, 1H), 7.54 (d, $J = 8.6$ Hz, 2H), 7.51–7.46 (m, 4H), 7.41 (t, $J = 7.4$ Hz, 1H), 7.29 (d, $J = 7.1$ Hz, 2H), 2.40 (s, 3H). ^{13}C NMR (126 MHz, DMSO- d_6) δ 159.84, 151.48, 150.55, 136.19, 133.12, 131.73, 131.40, 131.23, 131.12, 131.00, 129.65, 129.37, 125.80, 114.64, 14.55. MS (ESI): m/z 369.09 [M + H] $^+$.

3-Benzyl-6-(4-chlorophenyl)-5-methylthieno[2,3-*d*]pyrimidine-2,4(1*H*,3*H*)-dione (7d). **6b** (0.2 g, 0.7 mmol) and benzyl isocyanate (0.2 mL, 1.5 mmol) were reacted using a procedure similar to the synthesis of **7a**, affording compound **7d** (73 mg, yield 34%) as a white solid. ^1H NMR (500 MHz, DMSO- d_6) δ 12.38 (s, 1H), 7.53 (d, $J = 6.1$ Hz, 2H), 7.47 (d, $J = 7.6$ Hz, 2H), 7.31–7.24 (m, 5H), 5.04 (s, 2H), 2.43 (s, 3H). ^{13}C NMR (126 MHz, DMSO- d_6) δ 159.58, 151.07, 150.60, 137.91, 133.11, 131.70, 131.28, 130.82, 129.50, 128.79, 127.86, 127.49, 125.92, 114.20, 43.36, 14.56. HRMS, calculated for C $_{20}$ H $_{16}$ O $_2$ N $_2$ ClS [M + H] $^+$: 383.0616, found 383.0616.

6-(4-Chlorophenyl)-5-methyl-3-(4-(trifluoromethyl)benzyl)thieno[2,3-*d*]pyrimidine-2,4(1*H*,3*H*)-dione (7e). **6b** (0.2 g, 0.5 mmol) and 4-(trifluoromethyl)benzyl isocyanate (0.2 mL, 1.0 mmol) were reacted using a procedure similar to the synthesis of **7a**, affording compound **7e** (0.1 g, yield 44%) as a white solid. ^1H NMR (500 MHz, DMSO- d_6) δ 12.44 (s, 1H), 7.68 (d, $J = 6.8$ Hz, 2H), 7.56–7.44 (m, 6H), 5.12 (s, 2H), 2.42 (s, 3H). ^{13}C NMR (126 MHz, DMSO- d_6) δ 159.6, 151.3, 150.6, 142.7, 133.1, 131.7, 131.3, 131.1 (q, $J = 26.4$ Hz), 130.8, 129.4, 128.4, 126.0, 125.8, 124.4 (q, $J = 284.0$ Hz), 114.2, 43.2, 14.5. HRMS, calculated for C $_{21}$ H $_{15}$ O $_2$ N $_2$ ClF $_3$ S [M + H] $^+$: 451.0489, found 451.0489.

3-Benzyl-6-(3,4-dichlorophenyl)-5-methylthieno[2,3-*d*]pyrimidine-2,4(1*H*,3*H*)-dione (7f). **6c** (0.2 g, 0.5 mmol) and benzyl isocyanate (0.2 mL, 1.5 mmol) were reacted using a procedure similar to the synthesis of **7a**, affording compound **7f** (0.1 g, yield 48%) as a white solid. ^1H NMR (500 MHz, DMSO- d_6) δ 12.34 (s, 1H), 7.53 (dt, $J = 5.9, 2.7$ Hz, 2H), 7.27 (t, $J = 6.2$ Hz, 5H), 6.74 (d, $J = 4.5$ Hz, 1H), 5.00 (s, 2H), 4.16 (s, 3H). ^{13}C NMR (126 MHz, DMSO- d_6) δ 158.91, 150.35, 141.33, 137.47, 136.65, 130.71, 130.66, 130.41, 129.23, 128.66, 128.31, 127.47, 127.07, 120.90, 113.57, 111.82, 42.77, 33.69. HRMS, calculated for C $_{20}$ H $_{15}$ O $_2$ N $_2$ Cl $_2$ S [M + H] $^+$: 417.0226, found 417.0225.

3-Benzyl-6-(2,4-dichlorophenyl)-5-methylthieno[2,3-*d*]pyrimidine-2,4(1*H*,3*H*)-dione (7g). **6d** (0.2 g, 0.5 mmol) and benzyl isocyanate (0.2 mL, 1.5 mmol) were reacted using a procedure similar to the synthesis of **7a**, affording compound **7g** (82 mg, yield 39%) as a white solid. ^1H NMR (500 MHz, DMSO- d_6) δ 12.37 (s, 1H), 7.81 (d, $J = 2.0$ Hz, 1H), 7.56–7.49 (m, 2H), 7.33–7.29 (m, 4H), 7.26–7.23 (m, 1H), 5.04 (s, 2H), 2.18 (s, 3H). ^{13}C NMR (126 MHz, DMSO- d_6) δ 159.49, 151.85, 150.66, 137.91, 135.49, 135.01, 134.92, 133.15, 130.05, 129.79, 128.81, 127.91, 127.88, 127.53, 122.38, 113.26, 43.39, 14.68. HRMS, calculated for C $_{20}$ H $_{15}$ O $_2$ N $_2$ Cl $_2$ S [M + H] $^+$: 417.0226, found 417.0225.

3-Benzyl-5-methyl-6-(3-(trifluoromethyl)phenyl)thieno[2,3-*d*]pyrimidine-2,4(1*H*,3*H*)-dione (7h). **6e** (0.20 g, 0.50 mmol) and benzyl isocyanate (0.20 mL, 1.5 mmol) were reacted using a procedure similar to the synthesis of **7a**, affording compound **7h** (130 mg, yield 62%) as a white solid. ^1H NMR (500 MHz, DMSO- d_6) δ 12.46 (s, 1H), 7.75 (m, 4H), 7.32 (m, 4H), 7.26 (m, 1H), 5.06 (s, 2H), 2.45 (s, 3H). ^{13}C NMR (126 MHz, DMSO- d_6) δ 159.2, 151.0, 150.2, 137.5, 133.5, 133.2, 131.2, 130.3 (q, $J = 30.5$ Hz), 129.9, 129.6, 128.4, 127.4, 127.1, 125.6 (q, $J = 272.9$ Hz), 125.0, 122.9, 113.7, 42.9, 14.1. HRMS, calculated for C $_{21}$ H $_{16}$ O $_2$ N $_2$ F $_3$ S [M + H] $^+$: 417.0879, found 417.0879.

6-(Benzo[d][1,3]dioxol-5-yl)-3-benzyl-5-methylthieno[2,3-*d*]pyrimidine-2,4(1*H*,3*H*)-dione (7i). **6f** (0.20 g, 0.50 mmol) and benzyl isocyanate (0.2 mL, 1.5 mmol) were reacted using a procedure similar to the synthesis of **7a**, affording compound **7i** (38 mg, yield 20%) as a white solid. ^1H NMR (500 MHz, DMSO- d_6) δ 12.33 (s, 1H), 7.27 (dd, $J = 19.8, 6.8$ Hz, 5H), 7.01 (dd, $J = 10.2, 5.7$ Hz, 2H), 6.90 (t, $J = 6.3$ Hz, 1H), 6.08 (s, 2H), 5.04 (s, 2H), 2.39 (s, 3H). ^{13}C NMR (126 MHz, DMSO- d_6) δ 159.61, 150.67, 150.49, 148.16, 147.62, 137.95, 129.63, 128.80, 127.81, 127.48, 127.19, 126.31, 123.60, 114.03, 109.95, 109.19, 101.92, 43.31, 14.54. HRMS, calculated for C $_{21}$ H $_{17}$ O $_4$ N $_2$ S [M + H] $^+$: 393.0904, found 393.0897.

2-(Chloromethyl)-6-(4-chlorophenyl)-5-methylthieno[2,3-*d*]pyrimidin-4(1*H*)-one (8a). **6b** (0.33 g, 1.0 mmol) and 2-chloroacetonitrile (0.1 mL, 1.2 mmol) were diluted into HCl (4 N, 6 mL) in 1,4-dioxane (2 mL) and stirred for 1 h at room temperature. Subsequently, the reaction mixture was heated to 100 °C 12 h until

precipitation formed. After cooled down to room temperature, the reaction mixture was filtered and the precipitate was washed with *n*-hexane. The final product was purified with column chromatography with DCM:MeOH 10:1 (v/v). The product was obtained as a 195 mg white solid. Yield 60%. ¹H NMR (500 MHz, DMSO-*d*₆) δ 12.81 (s, 1H), 7.55 (m, 4H), 4.57 (s, 2H), 2.53 (s, 3H). ¹³C NMR (126 MHz, DMSO-*d*₆) δ 162.8, 158.8, 153.1, 133.1, 132.4, 131.5, 131.1, 130.9, 130.0, 129.1, 128.9, 123.0, 42.5, 14.3. HRMS, calculated for C₁₄H₁₁ON₂Cl₂S [M + H]⁺: 324.9964, found 324.9964.

2-Benzyl-6-(4-chlorophenyl)-5-methylthieno[2,3-*d*]pyrimidin-4(1*H*)-one (8b). **6b** (0.30 g, 1.0 mmol) was reacted with 2-phenylacetonitrile (0.20 g, 1.6 mmol) following similar procedure of synthesis of **8a** to afford **8b** (201 mg, 55%) as a white solid. ¹H NMR (500 MHz, DMSO-*d*₆) δ 12.6 (s, 1H), 7.6–7.5 (m, 4H), 7.4–7.3 (m, 4H), 7.3–7.2 (m, 1H), 4.0 (s, 2H), 2.5 (s, 3H) ppm. ¹³C NMR (126 MHz, DMSO-*d*₆) δ 163.8, 159.1, 157.1, 136.3, 132.9, 131.7, 131.0, 130.9, 130.8, 130.7, 129.7, 129.1, 128.9, 128.6, 126.9, 121.9, 56.9, 26.6 ppm. HRMS, calculated for C₂₀H₁₆ON₂ClS [M + H]⁺: 367.0666, found 367.0665.

2-Benzyl-6-(4-fluorophenyl)-5-methylthieno[2,3-*d*]pyrimidin-4(1*H*)-one (8c). **6g** (0.30 g, 1.1 mmol) was reacted with 2-(3-methoxyphenyl)acetonitrile (0.21 g, 1.4 mmol) following similar procedure of synthesis of **8a** to afford **8c** (127 mg, 32%) as a white solid. ¹H NMR (500 MHz, DMSO-*d*₆) δ 12.65 (s, 1H), 7.53 (dd, *J* = 8.7, 5.4 Hz, 2H), 7.37–7.29 (m, 6H), 7.25 (t, *J* = 6.7 Hz, 1H), 3.95 (s, 2H), 2.49 (s, 3H). ¹³C NMR (126 MHz, DMSO-*d*₆) δ 164.1, 162.3 (d, *J* = 246.0), 159.7, 157.4, 136.8, 131.9, 131.5, 129.7, 129.6, 129.4, 129.0, 127.4, 122.3, 116.4 (d, *J* = 21.4), 40.6, 14.7. HRMS, calculated for C₂₀H₁₆ON₂FS [M + H]⁺: 351.0962, found 351.0961.

6-(4-Chlorophenyl)-2-(3-methoxybenzyl)-5-methylthieno[2,3-*d*]pyrimidin-4(1*H*)-one (8d). **6g** (0.32 g, 1 mmol) was reacted with 2-phenylacetonitrile (0.21 g, 1.6 mmol) following similar procedure of synthesis of **8a** to afford **8d** (203 mg, 53%) as a white solid. ¹H NMR (500 MHz, DMSO-*d*₆) δ 12.6 (s, 1H), 7.6–7.4 (m, 4H), 7.2 (t, *J* = 7.8 Hz, 1H), 7.0–6.9 (m, 1H), 6.9 (d, *J* = 7.8 Hz, 1H), 6.8 (ddd, *J* = 8.4, 2.7, 1.0 Hz, 1H), 3.9 (s, 2H), 3.7 (s, 3H), 2.5 (s, 3H) ppm. ¹³C NMR (126 MHz, DMSO-*d*₆) δ 163.8, 159.3, 159.1, 156.9, 137.7, 132.8, 131.7, 131.0, 130.8, 130.7, 129.7, 129.6, 129.0, 128.8, 121.9, 121.0, 114.8, 112.2, 55.1, 54.9, 14.2. HRMS, calculated for C₂₁H₁₈O₂N₂ClS [M + H]⁺: 397.0772, found 397.0770.

Synthesis of **10a** was performed by following a reported method⁵⁰ (ethyl 2-amino-4-phenylthiophene-3-carboxylate, **10a**). An equimolar mixture of powdered sulfur (160 mg, 5.0 mmol) and morpholine (0.50 mL) was stirred until total dissolution of the sulfur. Then, ethyl cyanoacetate (0.60 mL, 5.0 mmol) and acetophenone (0.60 mL, 5 mmol) were added to the reaction mixture, which was stirred at room temperature for 18 h. After completion of the reaction, as monitored by TLC, the crude product was chromatographed on silica with CH₂Cl₂ to afford a white solid, yield 34%.

Ethyl 2-Amino-4-(4-chlorophenyl)thiophene-3-carboxylate (10b). **10b** was synthesized by following the same method as the preparation of **6a** using 1-(4-chlorophenyl)ethan-1-one (5 mmol) as a starting material. A white powder (250 mg) was obtained as the product with a yield of 18%.

3-Benzyl-5-phenylthieno[2,3-*d*]pyrimidine-2,4(1*H*,3*H*)-dione (11a). **11a** was prepared similarly to **7a** with a yield of 67%. ¹H NMR (500 MHz, DMSO-*d*₆) δ 12.43 (s, 1H), 7.44 (d, *J* = 6.4 Hz, 2H), 7.35 (q, *J* = 8.2, 7.3 Hz, 3H), 7.27 (d, *J* = 6.5 Hz, 4H), 7.21 (t, *J* = 6.4 Hz, 1H), 7.04 (s, 1H), 5.00 (s, 2H). ¹³C NMR (126 MHz, DMSO-*d*₆) δ 158.14, 152.69, 150.33, 138.92, 137.51, 134.95, 129.28, 128.32, 127.55, 127.47, 127.40, 127.01, 114.74, 111.16, 43.06. HRMS, calculated for C₁₉H₁₅O₂N₂S [M + H]⁺: 335.0849, found 335.0848.

3-Benzyl-5-(4-chlorophenyl)thieno[2,3-*d*]pyrimidine-2,4(1*H*,3*H*)-dione (11b). **11b** was prepared similarly to **7a** with a yield of 56%. ¹H NMR (500 MHz, DMSO-*d*₆) δ 12.42 (s, 1H), 7.46 (d, *J* = 8.4 Hz, 2H), 7.42 (d, *J* = 8.6 Hz, 2H), 7.31–7.19 (m, 5H), 7.08 (s, 1H), 5.00 (s, 2H). ¹³C NMR (126 MHz, DMSO-*d*₆) δ 158.13, 152.72, 150.22, 137.43, 137.39, 133.68, 132.26, 130.94, 128.24, 127.45, 127.35, 126.94, 121.99, 115.13, 43.03. HRMS, calculated for C₁₉H₁₄O₂N₂ClS [M + H]⁺: 369.0459, found 369.0459.

Preparation of Recombinant Human MIF2. The detailed procedures to produce recombinant human MIF2 were reported in our previous publications.⁴⁶ Gene sequences of the human MIF2 gene (Invitrogen) were adapted to bacterial expression. After subcloning into a pET20b(+) expression vector, IPTG-induced expression was performed in *E. coli* strain BL21(DE3). MIF2 protein was overproduced overnight, and harvested cells were resuspended and sonicated. The soluble fraction was purified using a Q sepharose column (GE Healthcare) with a gradient of NaCl. The fractions containing MIF2 were brought to 1.7 M ammonium sulfate and loaded on a phenyl sepharose column (GE Healthcare) and eluted with a gradient to 0 M ammonium sulfate in a 20 mM sodium phosphate buffer, pH 8.0. Finally, the proteins were purified by size exclusion chromatography on a Superdex75 column (GE Healthcare) in 20 mM sodium phosphate buffer, pH 8.0, with an elution volume characteristic for trimeric MIF2. The collected protein was concentrated using a VivaSpin centrifugation column with a molecular-weight cutoff at 5000 Da (Sartorius Stedim Biotech GmbH). Purified proteins were aliquoted, snap-frozen in liquid nitrogen, and stored at –80 °C. The purity of the obtained protein was tested by sodium dodecyl sulfate polyacrylamide gel electrophoresis (SDS-PAGE) and coomassie staining.

Tautomerase Assay. The MIF tautomerase activity and enzyme kinetics were measured by a previously described protocol.³⁵ The methods to study MIF2 enzyme activity were adapted from protocols to study MIF. Briefly, 10 μL of EDTA (20 mM) solution in demiwaterr was added into 180 μL of MIF2 solution (100 nM) in boric acid buffer (435 mM, pH 6.2), followed by the addition of 10 μL of the desired compound in DMSO or vehicle. This mixture was homogenized and preincubated at room temperature for 10 min. Subsequently, 50 μL of this enzyme–inhibitor mixture was mixed with 50 μL of phenylpyruvate solution (1 mM) in ammonium acetate buffer (50 mM, pH 6.0). The increase of UV absorbance at 300 nm over time represents MIF2 tautomerase activity. MIF2 tautomerase activity in the group containing blank DMSO dilution was set to 100%. Noncatalyzed conversion of the PP without the MIF presence was set to 0%. Data from the first 3 min were linear and used to calculate the conversion velocities. GraphPad Prism was employed for the calculation.

Cell Culture. Four different human lung cancer cell lines including A549 (ATCC-CCL-185), H1650 (ATCC-CRL-5883), H1299 (ATCC-CRL-5803), and HCC827 (ATCC-CRL-2868) were cultured in RPMI-1640 Medium (Gibco™ #61870-010) containing 10% (v/v) fetal bovine serum (FBS) and 100 U/mL penicillin/streptomycin (Gibco™ #10378016) at 37 °C with 5% CO₂ in humidified air.

Cell Proliferation Assay. Cell proliferation was measured with the CyQUANT Direct Cell Proliferation Assay Kit (Thermo Fisher, #C35011) by following the protocol. Cells were cultured in 96-well plates at a density of 1000 cells/well and treated with different concentrations of **5d** (0.25–10 μM) for 72 h. The cells were incubated with a detection reagent (100 μL) for 60 min at 37 °C with 5% CO₂. The fluorescence of each well was read at 485/535 nm by a plate reader (BioTek).

Clonogenic Assay. Cells were seeded in 12-well plates (1000 cells per well in 2 mL of the same medium used for cell proliferation assay) and incubated overnight. Corresponding inhibitors were added to the cell culture medium, and the cells were exposed to the treatment for 5 days. Subsequently, the medium was carefully removed and the cells were washed with PBS before they were fixed with 4% (v/v) paraformaldehyde for 20 min at room temperature. After removal of the fixation reagent, the cells were stained with 0.5% (w/v) crystal violet in the dark for 20 min. After washing, the image of stained cancer cell colonies in each well was photographed. To quantify the staining, 10% acetic acid was utilized to dissolve the colonies. The absorbance at a wavelength of 590 nm was measured to represent the relative cell number by comparing with the DMSO-treated group.

Tumor Spheroid Assay. A549 cells (1000 cells/well) were seeded onto a 96-well U bottom ultralow attachment plate (Corning). After 2 days of incubation without disturbance, the spheroid was

treated with indicated compound every 3 days. Images were captured, and the diameter of each tumor spheroid was measured on the indicated days post-treatment using an inverted microscope (Nikon Eclipse Ti) connected with NIS-Elements software. The data were analyzed and plotted with GraphPad Prism8.

ERK Phosphorylation Study.¹⁵ A549 cells were seeded into each well of a six-well plate in a density of 3×10^5 cells per well with 2 mL of RPMI-1640 medium containing 0.5% (v/v) FBS (Costar Europe, Badhoevedorp, The Netherlands), and 1% (v/v) penicillin/streptomycin solution (Corning). After overnight culturing, the cells were stimulated with MIF2 (100 ng/mL in FBS-free medium) or a mixture of MIF2 and different concentrations of **5d** for 15 min. Subsequently, the cells were washed with cold PBS and lysed using RIPA buffer containing PhosSTOP and protease inhibitor (PI) cocktail (Roche, Mannheim, Germany). After determination of the protein concentration of each sample using the BCA Protein Assay Kit (Pierce, Rockford IL), 20 μ g protein was loaded onto and separated by a precast 10% NuPAGE Bis-Tris gel (Invitrogen). The proteins in the gel were then transferred to a poly(vinylidene difluoride) (PVDF) membrane. After blocking with 5% (w/v) of skimmed milk for 1 h at room temperature and incubation with the appropriate primary antibody (pERK, #9101, Cell Signaling, 1:1000; ERK, #9102, Cell Signaling, 1:1000; GAPDH, #97166, Cell Signaling, 1:10 000) overnight at 4 °C, the membrane was treated with HRP-conjugated secondary antibodies and the protein bands were visualized with enhanced chemiluminescence (ECL) solution (GE Healthcare) and quantified with ImageJ software based on grayscale.

Flow Cytometry. For cell cycle analysis, A549 cells were seeded in six-well plates at a density of 1×10^5 per well. The next day, the cells were treated with **5d** or vehicle for 48 h. After the treatment, the cells were washed with PBS (3 \times) and then harvested after trypsinization. After centrifugation at 300g, the cells were incubated with a solution containing 20 μ g/mL propidium iodide (PI) (Sigma, P4864) and 0.1% (v/v) Triton-X100 (Sigma, T8787) for 15 min at room temperature. Fluorescence was detected by a Cytoflex flow cytometer (Beckman Coulter, Woerden, the Netherlands) immediately. A total of 30 000 cells were collected for each sample. Data were analyzed using FlowJo software (Tree Star, Ashland).

■ ASSOCIATED CONTENT

SI Supporting Information

The Supporting Information is available free of charge at <https://pubs.acs.org/doi/10.1021/acs.jmedchem.1c01598>.

Additional figures and schemes; HPLC assessment of purity and solubility for target compounds; tautomerase activity inhibition IC₅₀ curves; molecular modeling details; and analytical data (¹H NMR, ¹³C NMR, HRMS) (PDF)

Molecular formula strings (CSV)

■ AUTHOR INFORMATION

Corresponding Author

Frank J. Dekker – Chemical and Pharmaceutical Biology, Groningen Research Institute of Pharmacy (GRIP), University of Groningen, 9713 AV Groningen, The Netherlands; orcid.org/0000-0001-7217-9300; Phone: +31-5-3638030; Email: f.j.dekker@rug.nl; Fax: +31-5-3637953

Authors

Zhangping Xiao – Chemical and Pharmaceutical Biology, Groningen Research Institute of Pharmacy (GRIP), University of Groningen, 9713 AV Groningen, The Netherlands; orcid.org/0000-0003-0557-9843

Angelina Osipyan – Chemical and Pharmaceutical Biology, Groningen Research Institute of Pharmacy (GRIP),

University of Groningen, 9713 AV Groningen, The Netherlands

Shanshan Song – Chemical and Pharmaceutical Biology, Groningen Research Institute of Pharmacy (GRIP), University of Groningen, 9713 AV Groningen, The Netherlands; Molecular Pharmacology, Groningen Research Institute of Pharmacy (GRIP), University of Groningen, 9713 AV Groningen, The Netherlands

Deng Chen – Chemical and Pharmaceutical Biology, Groningen Research Institute of Pharmacy (GRIP), University of Groningen, 9713 AV Groningen, The Netherlands

Reinder A. Schut – Chemical and Pharmaceutical Biology, Groningen Research Institute of Pharmacy (GRIP), University of Groningen, 9713 AV Groningen, The Netherlands

Ronald van Merkerk – Chemical and Pharmaceutical Biology, Groningen Research Institute of Pharmacy (GRIP), University of Groningen, 9713 AV Groningen, The Netherlands

Petra E. van der Wouden – Chemical and Pharmaceutical Biology, Groningen Research Institute of Pharmacy (GRIP), University of Groningen, 9713 AV Groningen, The Netherlands

Robbert H. Cool – Chemical and Pharmaceutical Biology, Groningen Research Institute of Pharmacy (GRIP), University of Groningen, 9713 AV Groningen, The Netherlands

Wim J. Quax – Chemical and Pharmaceutical Biology, Groningen Research Institute of Pharmacy (GRIP), University of Groningen, 9713 AV Groningen, The Netherlands; orcid.org/0000-0002-5162-9947

Barbro N. Melgert – Molecular Pharmacology, Groningen Research Institute of Pharmacy (GRIP), University of Groningen, 9713 AV Groningen, The Netherlands; University Medical Center Groningen, Groningen Research Institute of Asthma and COPD, University of Groningen, 9713 GZ Groningen, The Netherlands

Gerrit J. Poelarends – Chemical and Pharmaceutical Biology, Groningen Research Institute of Pharmacy (GRIP), University of Groningen, 9713 AV Groningen, The Netherlands; orcid.org/0000-0002-6917-6368

Complete contact information is available at:

<https://pubs.acs.org/10.1021/acs.jmedchem.1c01598>

Author Contributions

All authors have given approval to the final version of the manuscript.

Funding

Z.X. and D.C. are funded by China Scholarship Council (grant nos.: 201706010341 for Z.X., 201907720019 for D.C.). A.O. was supported by funding from Marie Skłodowska-Curie Action (CoFund project 754425). S.S. was funded by Royalties Prof. Dr. H.W. Frijlink Scholarship from University of Groningen.

Notes

The authors declare no competing financial interest.

■ ACKNOWLEDGMENTS

The authors acknowledge Prof. Matthew R. Groves and Chao Wang from the Drug Design group, Groningen Research

Institute of Pharmacy, University of Groningen, for advices and help on the thermal shift assay.

ABBREVIATIONS USED

4-CPP, 4-chlorophenylpyruvate; 4-HPP, 4-hydroxyphenylpyruvate; 4-MPP, 4-methoxyphenylpyruvate; CD74, cluster of differentiation 74; CXCR4, chemokine receptor 4; D-DT, D-dopachrome tautomerase; DMF, *N,N*-dimethylformamide; DMSO, dimethyl sulfoxide; EDCl, 1-ethyl-3-(3-dimethylaminopropyl) carbodiimide hydrochloride; EDTA, ethylenediamine tetraacetic acid; ELISA, enzyme-linked immunosorbent assay; FID, fluorescent indicator displacement; HOBT, hydroxybenzotriazole; HTS, high-throughput screening; JAB1, c-Jun activation domain-binding protein-1; MAPK, mitogen-activated protein kinase; MIF, macrophage migration inhibitory factor; PP, phenylpyruvate; SAR, structure–activity relationship

REFERENCES

- (1) Bray, F.; Ferlay, J.; Soerjomataram, I.; Siegel, R. L.; Torre, L. A.; Jemal, A. Global cancer statistics 2018: GLOBOCAN estimates of incidence and mortality worldwide for 36 cancers in 185 countries. *Ca-Cancer J. Clin.* **2018**, *68*, 394–424.
- (2) Dagogo-Jack, I.; Shaw, A. T. Tumour heterogeneity and resistance to cancer therapies. *Nat. Rev. Clin. Oncol.* **2018**, *15*, 81–94.
- (3) Hahn, W. C.; Bader, J. S.; Braun, T. P.; Califano, A.; Clemons, P. A.; Druker, B. J.; Ewald, A. J.; Fu, H.; Jagu, S.; Kemp, C. J.; Kim, W.; Kuo, C. J.; Mcmanus, M.; Mills, G. B.; Mo, X.; Sahni, N.; Schreiber, S. L.; Talamas, J. A.; Tamayo, P.; Tyner, J. W.; Wagner, B. K.; Weiss, W. A.; Gerhard, D. S.; et al. An expanded universe of cancer targets. *Cell* **2021**, *184*, 1142–1155.
- (4) Penticuff, J. C.; Woolbright, B. L.; Sielecki, T. M.; Weir, S. J.; Taylor, J. A. MIF family proteins in genitourinary cancer: tumorigenic roles and therapeutic potential. *Nat. Rev. Urol.* **2019**, *16*, 318–328.
- (5) Soumoy, L.; Kindt, N.; Ghanem, G.; Saussez, S.; Journe, F. Role of macrophage migration inhibitory factor (Mif) in melanoma. *Cancers* **2019**, *11*, 529.
- (6) Cavalli, E.; Ciurleo, R.; Petralia, M. C.; Fagone, P.; Bella, R.; Mangano, K.; Nicoletti, F.; Bramanti, P.; Basile, M. S. Emerging role of the macrophage migration inhibitory factor family of cytokines in neuroblastoma. Pathogenic effectors and novel therapeutic targets? *Molecules* **2020**, *25*, 1194.
- (7) Coleman, A. M.; Rendon, B. E.; Zhao, M.; Qian, M.-W.; Bucala, R.; Xin, D.; Mitchell, R. A. Cooperative regulation of non-small cell lung carcinoma angiogenic potential by macrophage migration inhibitory factor and its homolog, D-dopachrome tautomerase. *J. Immunol.* **2008**, *181*, 2330–2337.
- (8) Charan, M.; Das, S.; Mishra, S.; Chatterjee, N.; Varikuti, S.; Kaul, K.; Misri, S.; Ahirwar, D. K.; Satoskar, A. R.; Ganju, R. K. Macrophage migration inhibitory factor inhibition as a novel therapeutic approach against triple-negative breast cancer. *Cell Death Dis.* **2020**, *11*, 774.
- (9) Zhang, M.; Yan, L.; Kim, J. A. Modulating mammary tumor growth, metastasis and immunosuppression by siRNA-induced MIF reduction in tumor microenvironment. *Cancer Gene Ther.* **2015**, *22*, 463–474.
- (10) Oliveira, C. S.; de Bock, C. E.; Molloy, T. J.; Sadeqzadeh, E.; Geng, X. Y.; Hersey, P.; Zhang, X. D.; Thorne, R. F. Macrophage migration inhibitory factor engages PI3K/Akt signalling and is a prognostic factor in metastatic melanoma. *BMC Cancer* **2014**, *14*, 630.
- (11) Leng, L.; Metz, C. N.; Fang, Y.; Xu, J.; Donnelly, S.; Baugh, J.; Delohery, T.; Chen, Y.; Mitchell, R. A.; Bucala, R. MIF signal transduction initiated by binding to CD74. *J. Exp. Med.* **2003**, *197*, 1467–1476.
- (12) Shi, X.; Leng, L.; Wang, T.; Wang, W.; Du, X.; Li, J.; McDonald, C.; Chen, Z.; Murphy, J. W.; Lolis, E.; Noble, P.; Knudson, W.; Bucala, R. CD44 is the signaling component of the macrophage migration inhibitory factor-CD74 receptor complex. *Immunity* **2006**, *25*, 595–606.
- (13) Jäger, B.; Klatt, D.; Plappert, L.; Golpon, H.; Lienenklaus, S.; Barbosa, P. D.; Schambach, A.; Prasse, A. CXCR4/MIF axis amplifies tumor growth and epithelial-mesenchymal interaction in non-small cell lung cancer. *Cell. Signalling* **2020**, *73*, No. 109672.
- (14) Mahalingam, D.; Patel, M.; Sachdev, J.; Hart, L.; Halama, N.; Ramanathan, R.; Sarantopoulos, J.; Liu, X.; Yazji, S.; Jäger, D.; Adib, D.; Kerschbaumer, R.; Yoon, M.; Manzur, G.; Starodub, A.; Sivarajan, K.; Wertheim, M.; Thambi, P.; Jones, M.; Goel, S.; Nemunaitis, J.; Tsimberidou, A. Safety and efficacy analysis of imalumab, an anti-oxidized macrophage migration inhibitory factor (oxMIF) antibody, alone or in combination with 5-fluorouracil/leucovorin (5-FU/LV) or panitumumab, in patients with metastatic colorectal cancer (mCRC). *Ann. Oncol.* **2016**, *27*, ii105.
- (15) Xiao, Z.; Chen, D.; Song, S.; Van Der Vlag, R.; Van Der Wouden, P. E.; Van Merkerk, R.; Cool, R. H.; Hirsch, A. K. H.; Melgert, B. N.; Quax, W. J.; Poelarends, G. J.; Dekker, F. J. 7-Hydroxycoumarins are affinity-based fluorescent probes for competitive binding studies of macrophage migration inhibitory factor. *J. Med. Chem.* **2020**, *63*, 11920–11933.
- (16) Illescas, O.; Pacheco-Fernández, T.; Laclette, J. P.; Rodriguez, T.; Rodriguez-Sosa, M. Immune modulation by the macrophage migration inhibitory factor (MIF) family: D-dopachrome tautomerase (DDT) is not (always) a backup system. *Cytokine* **2020**, *133*, 155121.
- (17) Merk, M.; Zierow, S.; Leng, L.; Das, R.; Du, X.; Schulte, W.; Fan, J.; Lue, H.; Chen, Y.; Xiong, H.; Chagnon, F.; Bernhagen, J.; Lolis, E.; Mor, G.; Lesur, O.; Bucala, R. The D-dopachrome tautomerase (DDT) gene product is a cytokine and functional homolog of macrophage migration inhibitory factor (MIF). *Proc. Natl. Acad. Sci. U.S.A.* **2011**, *108*, E577–E585.
- (18) Sugimoto, H.; Taniguchi, M.; Nakagawa, A. I.; et al. Crystal structure of human D-dopachrome tautomerase, a homologue of macrophage migration inhibitory factor, at 1.54 Å resolution. *Biochemistry* **1999**, *38*, 3268–3279.
- (19) Rajasekaran, D.; Zierow, S.; Syed, M.; Bucala, R.; Bhandari, V.; Lolis, E. J. Targeting distinct tautomerase sites of D-DT and MIF with a single molecule for inhibition of neutrophil lung recruitment. *FASEB J.* **2014**, *28*, 4961–4971.
- (20) Bernhagen, J.; Krohn, R.; Lue, H.; Gregory, J. L.; Zernecke, A.; Koenen, R. R.; Dewor, M.; Georgiev, I.; Schober, A.; Leng, L.; Kooistra, T.; Fingerle-Rowson, G.; Ghezzi, P.; Kleemann, R.; McColl, S. R.; Bucala, R.; Hickey, M. J.; Weber, C. MIF is a noncognate ligand of CXC chemokine receptors in inflammatory and atherogenic cell recruitment. *Nat. Med.* **2007**, *13*, 587–596.
- (21) Weber, C.; Kraemer, S.; Drechsler, M.; Lue, H.; Koenen, R. R.; Kapurniotu, A.; Zernecke, A.; Bernhagen, J. Structural determinants of MIF functions in CXCR2-mediated inflammatory and atherogenic leukocyte recruitment. *Proc. Natl. Acad. Sci. U.S.A.* **2008**, *105*, 16278–16283.
- (22) Pantouris, G.; Syed, M. A.; Fan, C.; Rajasekaran, D.; Cho, T. Y.; Rosenberg, E. M.; Bucala, R.; Bhandari, V.; Lolis, E. J. An analysis of MIF structural features that control functional activation of CD74. *Chem. Biol.* **2015**, *22*, 1197–1205.
- (23) Pantouris, G.; Khurana, L.; Ma, A.; Skeens, E.; Reiss, K.; Batista, V. S.; Lisi, G. P.; Lolis, E. J. Regulation of MIF enzymatic activity by an allosteric site at the central solvent channel. *Cell Chem. Biol.* **2020**, *27*, 740–750.
- (24) Bloom, J.; Sun, S.; Al-Abed, Y. MIF, a controversial cytokine: a review of structural features, challenges, and opportunities for drug development. *Expert Opin. Ther. Targets* **2016**, *20*, 1463–1475.
- (25) Al-Abed, Y.; VanPatten, S. MIF as a disease target: ISO-1 as a proof-of-concept therapeutic. *Future Med. Chem.* **2011**, *3*, 45–63.
- (26) Meyer-Siegler, K. L.; Iczkowski, K. A.; Leng, L.; Bucala, R.; Vera, P. L. Inhibition of macrophage migration inhibitory factor or its receptor (CD74) attenuates growth and invasion of DU-145 prostate cancer cells. *J. Immunol.* **2006**, *177*, 8730–8739.
- (27) Dziedzic, P.; Cisneros, J. A.; Robertson, M. J.; Hare, A. A.; Danford, N. E.; Baxter, R. H. G.; Jorgensen, W. L. Design, synthesis,

and protein crystallography of biaryltriazoles as potent tautomerase inhibitors of macrophage migration inhibitory factor. *J. Am. Chem. Soc.* **2015**, *137*, 2996–3003.

(28) Trivedi-Parmar, V.; Robertson, M. J.; Cisneros, J. A.; Krimmer, S. G.; Jorgensen, W. L. Optimization of pyrazoles as phenol surrogates to yield potent inhibitors of macrophage migration inhibitory factor. *ChemMedChem* **2018**, *13*, 1092–1097.

(29) Xiao, Z.; Song, S.; Chen, D.; Merkerk, R.; Wouden, P. E.; Cool, R. H.; Quax, W. J.; Poelarends, G. J.; Melgert, B. N.; Dekker, F. J. Proteolysis targeting chimera (PROTAC) for macrophage migration inhibitory factor (MIF) has anti-proliferative activity in lung cancer cells. *Angew. Chem., Int. Ed.* **2021**, *60*, 17514–17521.

(30) Tilstam, P. V.; Pantouris, G.; Corman, M.; Andreoli, M.; Mahboubi, K.; Davis, G.; Du, X.; Leng, L.; Lolis, E.; Bucala, R. A selective small-molecule inhibitor of macrophage migration inhibitory factor-2 (MIF-2), a MIF cytokine superfamily member, inhibits MIF-2 biological activity. *J. Biol. Chem.* **2019**, *294*, 18522–18531.

(31) Cho, Y.; Crichlow, G. V.; Vermeire, J. J.; Leng, L.; Du, X.; Hodsdon, M. E.; Bucala, R.; Cappello, M.; Gross, M.; Gaeta, F.; Johnson, K.; Lolis, E. J. Allosteric inhibition of macrophage migration inhibitory factor revealed by ibudilast. *Proc. Natl. Acad. Sci. U.S.A.* **2010**, *107*, 11313–11318.

(32) Pantouris, G.; Bucala, R.; Lolis, E. J. Structural plasticity in the C-terminal region of macrophage migration inhibitory factor-2 is associated with an induced fit mechanism for a selective inhibitor. *Biochemistry* **2018**, *57*, 3599–3605.

(33) Ouertatani-Sakouhi, H.; Liu, M.; El-Turk, F.; Cuny, G. D.; Glicksman, M. A.; Lashuel, H. Kinetic-based high-throughput screening assay to discover novel classes of macrophage migration inhibitory factor inhibitors. *J. Biomol. Screening* **2010**, *15*, 347–358.

(34) Rosengren, E.; Åman, P.; Thelin, S.; Hansson, C.; Ahlfors, S.; Björk, P.; Jacobsson, L.; Rorsman, H. The macrophage migration inhibitory factor MIF is a phenylpyruvate tautomerase. *FEBS Lett.* **1997**, *417*, 85–88.

(35) Xiao, Z.; Fokkens, M.; Chen, D.; Kok, T.; Proietti, G.; van Merkerk, R.; Poelarends, G. J.; Dekker, F. J. Structure-activity relationships for binding of 4-substituted triazole-phenols to macrophage migration inhibitory factor (MIF). *Eur. J. Med. Chem.* **2020**, *186*, 111849–111862.

(36) Zhang, J.-H.; Chung, T. D. Y.; Oldenburg, K. R. A simple statistical parameter for use in evaluation and validation of high throughput screening assays. *J. Biomol. Screening* **1999**, *4*, 67–73.

(37) Lubetsky, J. B.; Swope, M.; Dealwis, C.; Blake, P.; Lolis, E. Pro-1 of macrophage migration inhibitory factor functions as a catalytic base in the phenylpyruvate tautomerase activity. *Biochemistry* **1999**, *38*, 7346–7354.

(38) Ishikawa, M.; Hashimoto, Y. Improvement in aqueous solubility in small molecule drug discovery programs by disruption of molecular planarity and symmetry. *J. Med. Chem.* **2011**, *54*, 1539–1554.

(39) Feng, W.; Teo, X. Y.; Novera, W.; Ramanujulu, P. M.; Liang, D.; Huang, D.; Moore, P. K.; Deng, L. W.; Dymock, B. W. Discovery of new H₂S releasing phosphordithioates and 2,3-dihydro-2-phenyl-2-sulfanylenebenzo[d][1,3,2]oxazaphospholes with improved antiproliferative activity. *J. Med. Chem.* **2015**, *58*, 6456–6480.

(40) Guo, D.; Guo, J.; Yao, J.; Jiang, K.; Hu, J.; Wang, B.; Liu, H.; Lin, L.; Sun, W.; Jiang, X. D-dopachrome tautomerase is over-expressed in pancreatic ductal adenocarcinoma and acts cooperatively with macrophage migration inhibitory factor to promote cancer growth. *Int. J. Cancer* **2016**, *139*, 2056–2067.

(41) Pasupuleti, V.; Du, W.; Gupta, Y.; Yeh, I. J.; Montano, M.; Magi-Galuzzi, C.; Welford, S. M. Dysregulated D-dopachrome tautomerase, a hypoxiainducible factor-dependent gene, cooperates with macrophage migration inhibitory factor in renal tumorigenesis. *J. Biol. Chem.* **2014**, *289*, 3713–3723.

(42) Trivedi-Parmar, V. C.; Jorgensen, W. L. Advances and insights for small molecule inhibition of macrophage migration inhibitory factor. *J. Med. Chem.* **2018**, *61*, 8104–8119.

(43) Vinci, M.; Gowan, S.; Boxall, F.; Patterson, L.; Zimmermann, M.; Court, W.; Lomas, C.; Mendiola, M.; Hardisson, D.; Eccles, S. A. Advances in establishment and analysis of three-dimensional tumor spheroid-based functional assays for target validation and drug evaluation. *BMC Biol.* **2012**, *10*, No. 29.

(44) Kobold, S.; Merk, M.; Hofer, L.; Peters, P.; Bucala, R.; Endres, S. The macrophage migration inhibitory factor (MIF)-homologue D-dopachrome tautomerase is a therapeutic target in a murine melanoma model. *Oncotarget* **2014**, *5*, 103–107.

(45) Williams, G. H.; Stoerber, K. The cell cycle and cancer. *J. Pathol.* **2012**, *226*, 352–364.

(46) Song, S.; Liu, B.; Habibie, H.; van den Bor, J.; Smit, M. J.; Gosens, R.; Wu, X.; Brandsma, C.-A.; Cool, R. H.; Haisma, H. J.; Poelarends, G. J.; Melgert, B. N. D-dopachrome tautomerase contributes to lung epithelial repair via atypical chemokine receptor 3-dependent Akt signaling. *EBioMedicine* **2021**, *68*, No. 103412.

(47) Zhang, S.; Li, G.; Liu, H.; Wang, Y.; Cao, Y.; Zhao, G.; Tang, Z. Bio-inspired enantioselective full transamination using readily available cyclodextrin. *RSC Adv.* **2017**, *7*, 4203–4208.

(48) Eleftheriadis, N.; Poelman, H.; Leus, N. G. J.; Honrath, B.; Neochoritis, C. G.; Dolga, A.; Dömling, A.; Dekker, F. J. Design of a novel thiophene inhibitor of 15-lipoxygenase-1 with both anti-inflammatory and neuroprotective properties. *Eur. J. Med. Chem.* **2016**, *122*, 786–801.

(49) Sasaki, S.; Cho, N.; Nara, Y.; Harada, M.; Endo, S.; Suzuki, N.; Furuya, S.; Fujino, M. Discovery of a thieno[2,3-d]pyrimidine-2,4-dione bearing a p-methoxyureidophenyl moiety at the 6-position: A highly potent and orally bioavailable non-peptide antagonist for the human luteinizing hormone-releasing hormone receptor. *J. Med. Chem.* **2003**, *46*, 113–124.

(50) Fyfe, T. J.; Zarzycka, B.; Lim, H. D.; Kellam, B.; Mistry, S. N.; Katrich, V.; Scammells, P. J.; Lane, J. R.; Capuano, B. A thieno[2,3-d]pyrimidine scaffold is a novel negative allosteric modulator of the dopamine D₂ receptor. *J. Med. Chem.* **2019**, *62*, 174–206.